Economic Geology, v. 110, pp. 557–574

SCIENTIFIC COMMUNICATIONS

GEOLOGY, Re-Os AGES, SULFUR AND LEAD ISOTOPES OF THE DIYANQINAMU PORPHYRY Mo DEPOSIT, INNER MONGOLIA, NE CHINA

Cheng-Biao Leng,[1, 2,†] Xing-Chun Zhang,[1] Zhi-Long Huang,[1,†] Qiu-Yue Huang,[2] Shou-Xu Wang,[3] De-Yun Ma,[3] Tai-Yi Luo,[1] Chao Li,[4] and Wen-Bo Li[5]

[1] *State Key Laboratory of Ore Deposit Geochemistry, Institute of Geochemistry, Chinese Academy of Sciences, Guiyang 550002, China*

[2] *ARC Centre of Excellence in Ore Deposits (CODES), School of Physical Sciences, University of Tasmania, Hobart 7001, Australia*

[3] *Shandong Gold Group Co. Ltd., Jinan 250014, China*

[4] *National Research Center of Geoanalysis, Beijing 100037, China*

[5] *Laboratory of Crustal and Orogenic Evolution, Peking University, Beijing 100871, China*

Abstract

The Diyanqinamu porphyry Mo deposit in the southern Greater Khingan Range of the Central Asian orogenic belt contains 800 million metric tons (Mt) of ore with an average grade of 0.097% molybdenum. The deposit is hosted in Late Jurassic volcanic rocks of tuff, andesite, and volcanic breccia. Multiple-stage hydrothermal activities have resulted in propylitic, phyllic, and argillic alteration in this deposit. Five stages (I–V) of hydrothermal activity are identified. Stage I is represented by a mineral assemblage of epidote, chlorite, and magnetite, with some discontinuous barren veinlets of quartz + K-feldspar ± fluorite ± magnetite ± epidote ± chlorite. Stage II is marked by occurrence of quartz + fluorite + molybdenite + magnetite ± pyrite ± sericite ± siderite veinlets/veins with phyllic halos. Stage III consists of fluorite + siderite + quartz + molybdenite + pyrite ± ankerite ± calcite ± chalcopyrite veins that are commonly related to phyllic alteration and dissemination of fluorite in the altered rocks. Stage IV has an assemblage of fluorite + quartz + pyrite ± ankerite ± calcite ± molybdenite ± chalcopyrite ± sphalerite ± galena in coarse veins (10–20 mm wide). Stage V consists of narrow (≤5-mm wide) veinlets of calcite + fluorite + pyrite ± quartz. Molybdenite mainly occurs in Stages II and III.

Re-Os dating results for molybdenite samples from these two stages yielded an isochron age of 156.2 ± 4.2 Ma (2σ, MSWD = 0.96, n = 10). Most molybdenite samples have high $\delta^{34}S$ values (≥8.4‰) relative to other sulfide minerals (i.e., galena, sphalerite, pyrite, and chalcopyrite) of Stages II to V ($\delta^{34}S$ = 2.5–8.3‰, n = 22). Molybdenite also has low $^{207}Pb/^{204}Pb$ and $^{208}Pb/^{204}Pb$ ratios relative to other sulfide minerals although there are minor overlaps. In a diagram of $^{206}Pb/^{204}Pb$ versus $^{207}Pb/^{204}Pb$, these Pb isotope data display a positive trend transecting the growth curves of crustal lead, which could be invoked by mixing of crustal and mantle sources with distinct Pb isotopes. In combination with the S isotope data and mineral paragenesis, we suggest that magmas were the main source of molybdenum, whereas other metals (i.e., Pb, Zn, and Cu) were possibly sourced from the country rocks.

Introduction

The Diyanqinamu porphyry Mo deposit is located in the southern Greater Khingan Range of northeast China (Figs. 1, 2). The Greater Khingan Range is considered to be the easternmost segment of the Paleozoic Central Asian orogenic belt (Jahn et al., 2000), which is also known as the Altaid tectonic collage (Sengör et al., 1993). The Central Asian orogenic belt was formed mainly as a result of progressive subduction of the Paleo-Asian Ocean and amalgamation of various arcs and terranes during the Paleozoic (e.g., Xiao et al., 2003; Windley et al., 2007). It is characterized by extensive juvenile crustal growth from the Phanerozoic to Mesozoic (e.g., Jahn et al., 2000; Wu et al., 2000; Kovalenko et al., 2004). The Central Asian orogenic belt is also one of the most important metallogenic belts in the world and hosts numerous Cu, Au, Pb, and Zn ore deposits ranging in age from Neoproterozoic to Cretaceous (e.g., Zhang et al., 1999; Xiao et al., 2003, 2009; Berzina et al., 2005; Shen et al., 2012; Goldfarb et al., 2013; Seltmann et al., 2014).

Over 30 porphyry-type deposits are emplaced in the Greater Khingan Range (Ge et al., 2007; Zhang et al., 2009; Shen et al., 2010; Nie and Jiang, 2011; Sun et al., 2012; Zhou et al., 2012; Ma et al., 2013) associated with extensive felsic magmatic activities during the Late Permian to the Early Cretaceous (e.g., Nie et al., 2007; Chen et al., 2008; Wu et al., 2008; Zhang et al., 2009; Wan et al., 2009; Shen et al., 2010; Nie and Jiang, 2011; Ma et al., 2013). Some of these porphyry Mo-(Cu-W) deposits, such as Chehugou, Jiguanshan, and Xiaoxigou, occur in the Xilamulun tectonic-metallogenic belt (Fig. 1; Zhang et al., 2009; Wu et al., 2011; Ma et al., 2013; Seltmann et al., 2014), whereas other porphyry Mo-(W) deposits, including Ulandler and Bogda Uul, occur in the Chagan Obo-Aoyoute-Chaobulen tectono-magmatic belt (Figs. 1, 2; Nie et al., 2007; Nie and Jiang, 2011).

The Diyanqinamu porphyry Mo deposit is a newly discovered deposit in the Chagan Obo-Aoyoute-Chaobulen belt (Figs. 1, 2) and contains approximately 800 million metric tons (Mt) of ore with an average grade of 0.097% Mo, using

† Corresponding authors: e-mail, lengchengbiao@vip.gyig.ac.cn; huangzhilong@vip.gyig.ac.cn

0361-0128/15/4296/557-18

Submitted: January 17, 2014
Accepted: June 18, 2014

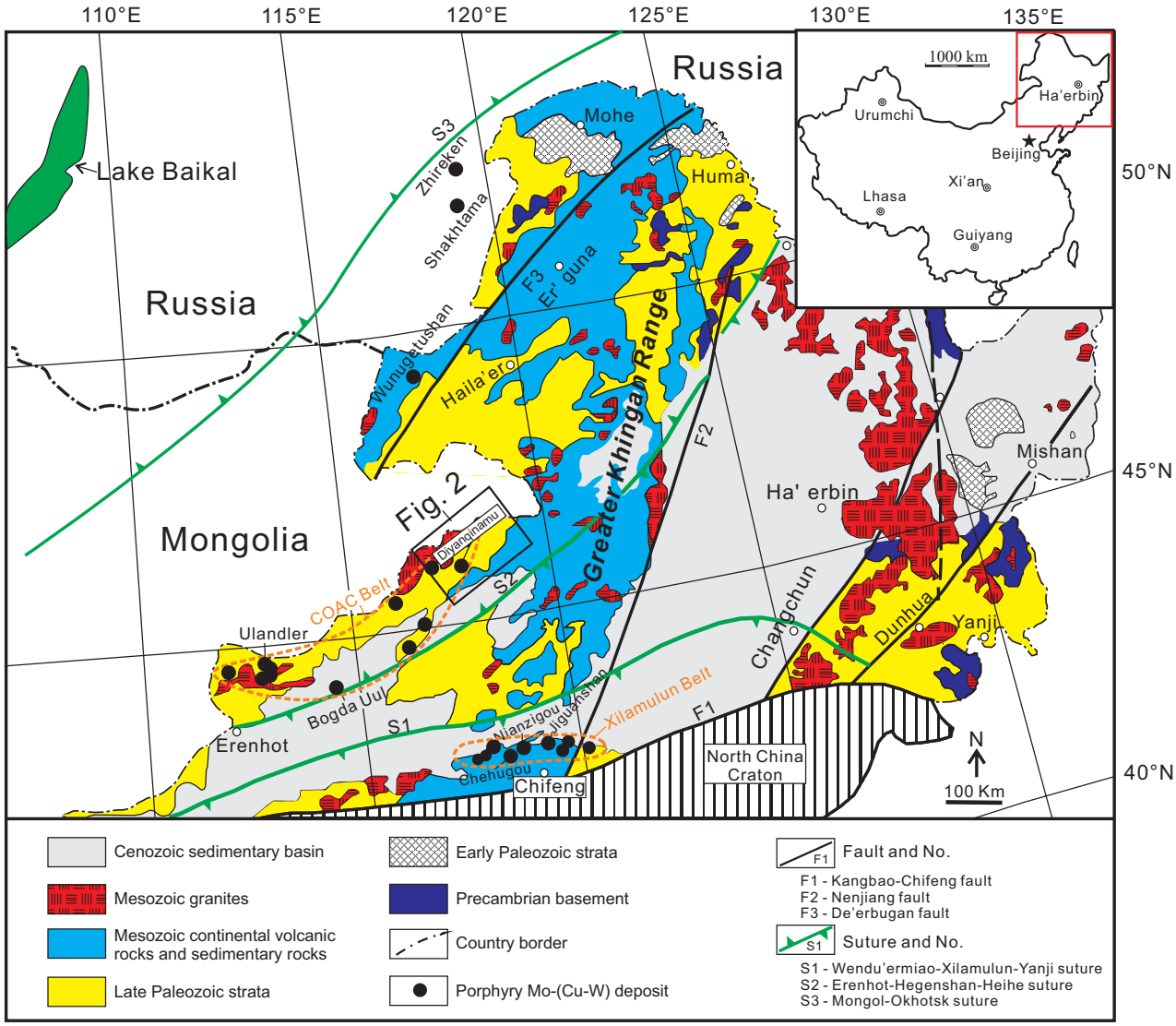

FIG. 1. Simplified geologic map of the Greater Khingan Range and its adjacent areas (modified from Shen et al., 2010, and Zhou et al., 2012), highlighting the tectonic framework and porphyry Mo-(Cu-W) deposit locations. COAC = Chagan Obo-Aoyoute-Chaobulen tectono-magmatic belt. Inset shows the studied area.

a 0.06% Mo cutoff. Approximately 148,000 m diamond drilling had been completed at Diyanqinamu over the past several years. Nie and Hou (2010) presented a short report on this deposit, and Yan et al. (2012) built a model of hydrothermal alteration zonation using near-infrared spectroscopy and Gemcom Surpac three dimensional (3-D) modeling software. More recently, Sun et al. (2014) obtained identical zircon U-Pb ages of 156 ± 2 Ma (2σ) for two granite samples from this deposit. In this contribution, we provide a detailed description of the Diyanqinamu deposit, together with new molybdenite Re-Os ages and S and Pb isotope compositions. Our results are used to constrain the timing of mineralization and possible sources of sulfur and metals in the Diyanqinamu deposit.

Geologic Background

The Greater Khingan Range, NE China, extends northeastward from Chifeng in Inner Mongolia to Mohe in Heilongjiang Province, with a length of 1,400 km and a width of 200 to 300 km (Fig. 1). It is located between the Siberian and North China cratons and is bounded by the Mongol-Okhotsk suture to the north, the Kangbao-Chifeng fault to south, the Neijing fault to the east, and the international border between China and Mongolia to the west (Fig. 1). Four different tectono-stratigraphic units are distributed in the Greater Khingan Range, including: (1) Precambrian metamorphic basement, which is thought to be composed of Neoarchean to Neoproterozoic metamorphic rocks including schists, gneisses, and granulites; (2) early Paleozoic weakly metamorphosed volcanic and sedimentary rocks, consisting of schist, slate, marble, and meta-andesite with typical continental margin and arc accretion features; (3) widespread late Paleozoic (mainly Permian) weakly metamorphosed volcanic and sedimentary rocks, which are similar to those of the early Paleozoic unit but with lower metamorphic grades; and (4) Jurassic and Cretaceous

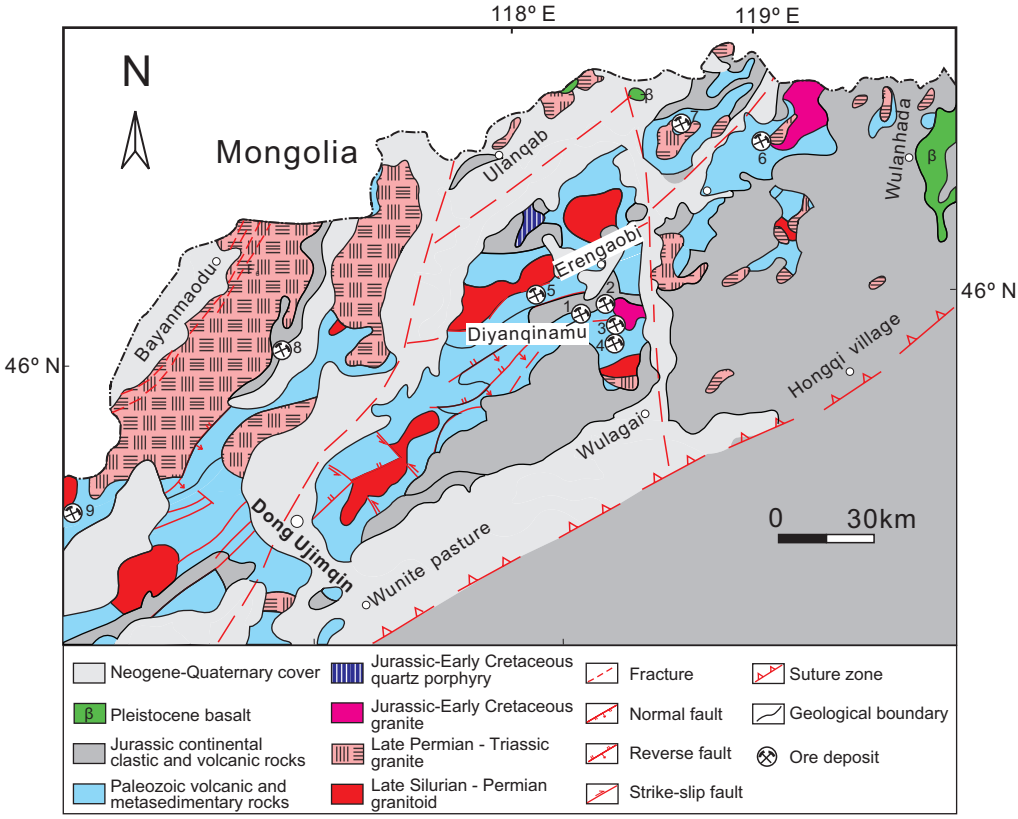

FIG. 2. Sketch geologic map of the Dong Ujimqin region, Inner Mongolia (modified from Zhang, 2008), highlighting the distribution of granitoid intrusions and some ore deposits, including 1 = Diyanqinamu porphyry Mo, 2 = Dasaituo skarn Pb-Zn-Ag, 3 = Chaganaobao skarn Fe-Zn, 4 = Manteaobao skarn Zn, 5 = Jilinbaolige epithermal Ag-Au, 6 = Aerhada epithermal Pb-Zn-Ag, 7 = Chaobuleng skarn Fe-Zn, 8 =Shamai epithermal W, 9 =Aoyoute porphyry Cu.

continental intermediate-felsic volcanic and sedimentary rocks (Liu et al., 2004; Zhou et al., 2012).

In the Dong Ujimqin region (Fig. 2), Ordovician-Permian volcanic and metasedimentary strata are composed of sericite schist, slate, meta-siltstone, argillite, and quartzite, which are intercalated with mafic-intermediate volcanic rocks (Inner Mongolian Bureau of Geology and Mineral Resources, 1991; Zhang, 2008; Nie and Jiang, 2011). Jurassic strata mainly consist of continental clastic rocks and intermediate-felsic volcanic rocks, with thickness ranging from 2,000 to 7,430 m (Nie et al., 2007; Nie and Jiang, 2011), and unconformably overlie the Paleozoic strata. In this region, several orogenic processes during the Late Silurian to the Early Cretaceous led to an ENE- to NNE-trending tectonic fabric (Fig. 2; Nie et al., 2007). Numerous granite and granodiorite batholiths, stocks, and dikes were emplaced along fracture zones parallel to this fabric in the northern part of this region (Fig. 2; Nie and Jiang, 2011). Their ages cluster in three main episodes: 325 to 275, 235 to 224, and 137 to 131 Ma (Zhao et al., 1994; Hong et al., 2003; Jin et al., 2005; Nie et al., 2007a; Zhang, 2008; Nie and Jiang, 2011). The latter two episodes of intrusions are spatially and temporally related to several styles of mineralization, including hydrothermal Au-Ag-Pb-Zn veins, Fe-Zn-Pb-Ag skarns, and porphyry Mo-(W-Cu) deposits (Fig. 2; Nie et al., 2007; Zhang, 2008; Nie and Jiang, 2011).

Deposit Geology

Host rocks

The Diyanqinamu deposit is mostly concealed by Quaternary overburden and is mainly hosted in Late Jurassic volcanic rocks of the Chagannuoer Formation, which unconformably overlie the Middle Ordovician Hanwula Formation (Fig. 3). The Chagannuoer Formation is composed of a series of intermediate-felsic lavas (mainly andesite and minor rhyolite) and volcaniclastic rocks including tuff and volcanic breccia with a thickness of over 1,000 m. Mineralized andesite has a zircon U-Pb age of 165 ± 3 Ma (2σ, n = 11, MSWD = 1.8; Shandong Gold Group Co. Ltd., unpub. data, 2012). The main components of the Chagannuoer Formation are described below.

Tuff generally contains about 45 vol % of crystal fragments (0.05–1 mm) consisting of feldspar (25 vol %) and quartz (15 vol %), minor lithic fragments (5 vol %), and 55 vol % of matrix (Figs. 4a, 5a). The matrix consists of microcrystalline feldspar and quartz (25 vol %), volcanic glass (15 vol %), clay minerals (10 vol %), and opaque minerals (5 vol %).

Volcanic breccia is mainly composed of 40 vol % of lithic fragments (2–20 mm) and over 50 vol % of volcanic ash (Fig. 4b, c). Lithic fragments include 20 vol % of andesitic fragments and 20 vol % of felsic fragments. The matrix is composed of more or less altered volcanic ash which is mainly composed of cryptocrystalline quartz and feldspar.

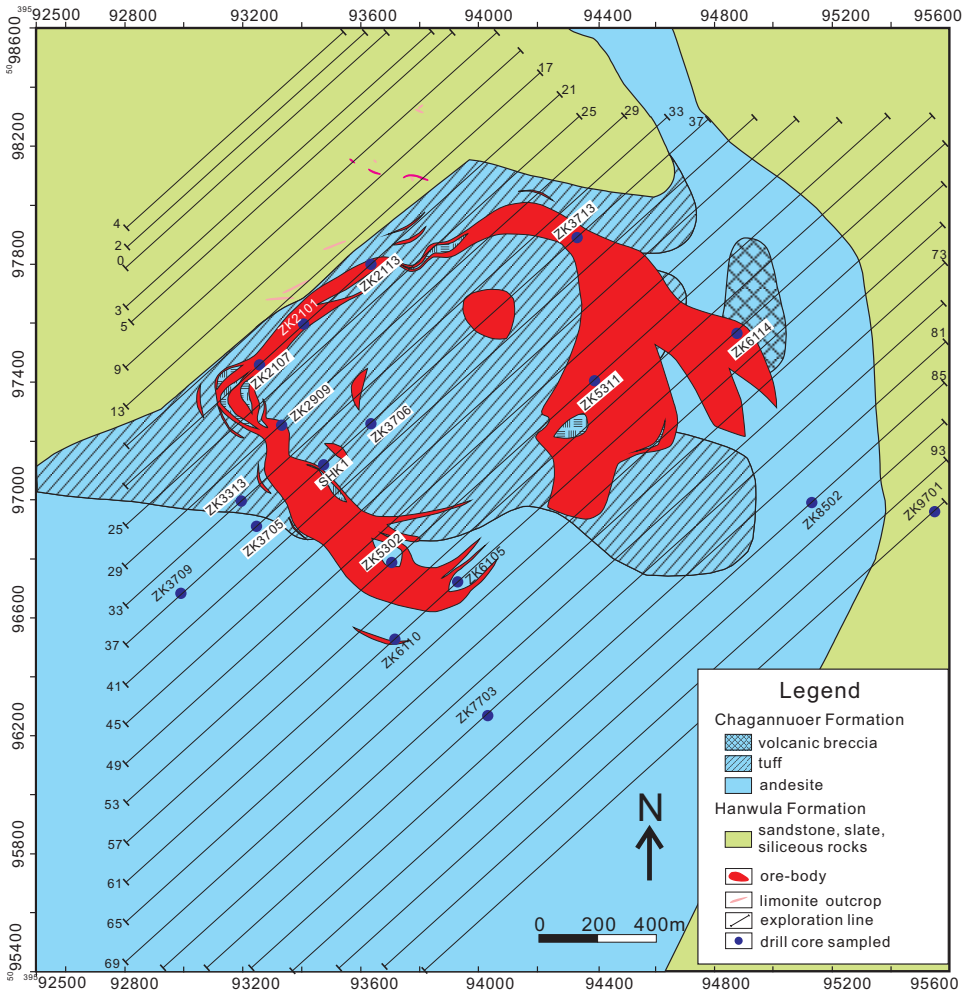

FIG. 3. Simplified bedrock geologic of the Diyanqinamu porphyry Mo deposit (modified from unpub. map provided by Shandong Gold Group Co. Ltd., 2012).

Andesite is made up of phenocrysts (30–35 vol %) and groundmass (65–70 vol %; Fig. 4d). Phenocrysts include 25 to 30 vol % of 0.1 to 1 mm tabular plagioclase and 5 vol % of 1 to 2 mm hornblende and biotite (Fig. 5b, c). The groundmass comprises very fine grained plagioclase and K-feldspar.

Rhyolite consists of about 5 vol % of phenocrysts with abundant 0.1 to 0.6 mm K-feldspar and minor 0.25 to 1.0 mm quartz, and about 95 vol % of groundmass of cryptocrystalline felsic minerals (Fig. 4e).

Intrusions

No intrusions are exposed at surface near the deposit, but several intrusive stocks and/or dikes have been intersected in drill holes (e.g., ZK3706, ZK8502, and ZK9701). They include quartz monzonite porphyry (Fig. 4g), dacitic porphyry (Fig. 4h), K-feldspar granite, and diorite. These intrusions have generally undergone variable degrees of phyllic and/or propylitic alteration, which is locally accompanied by weak mineralization (see below). No crosscutting relationships have been observed either among the intrusions or between the intrusions and orebodies in drill core, so their genetic relationship with mineralization is still an open question.

Quartz monzonite porphyry intrusions are observed in drill hole ZK8502 from 684 m to 725.9 m, and locally in drill holes ZK3706 and ZK6114. It contains 1–4 mm phenocrysts of K-feldspar (~20 vol %), plagioclase (10–15 vol %), and quartz (5–10 vol %), in a groundmass (55–65 vol %) of felsic minerals and minor biotite. Accessory minerals include magnetite, zircon, apatite and rutile.

Dacitic porphyry dikes are found in drill holes ZK3706, ZK3313, and ZK5311. This lithology comprises 10 to 20 vol % of plagioclase phenocrysts and 80 to 90 vol % of felsic groundmasses. This rock has undergone moderate amounts of silicic and phyllic alteration (Fig. 4h).

A K-feldspar granite stock was encountered in drill hole ZK9701 from 504 to 692 m. It is medium to coarse grained and is composed of 1 to 3 mm smoky quartz (30 vol %), pink tabular K-feldspar (40 vol %), tabular plagioclase (20 vol %), and minor biotite and hornblende, with accessory zircon, magnetite, and apatite. It has a zircon U-Pb age of 156 ± 2 Ma (2σ, n = 21, MSWD = 0.90; Sun et al., 2014).

Diorite dikes were intersected in some drill holes on exploration lines 21, 25, and 29 in the northwestern part of the deposit and are composed of hornblende (45 vol

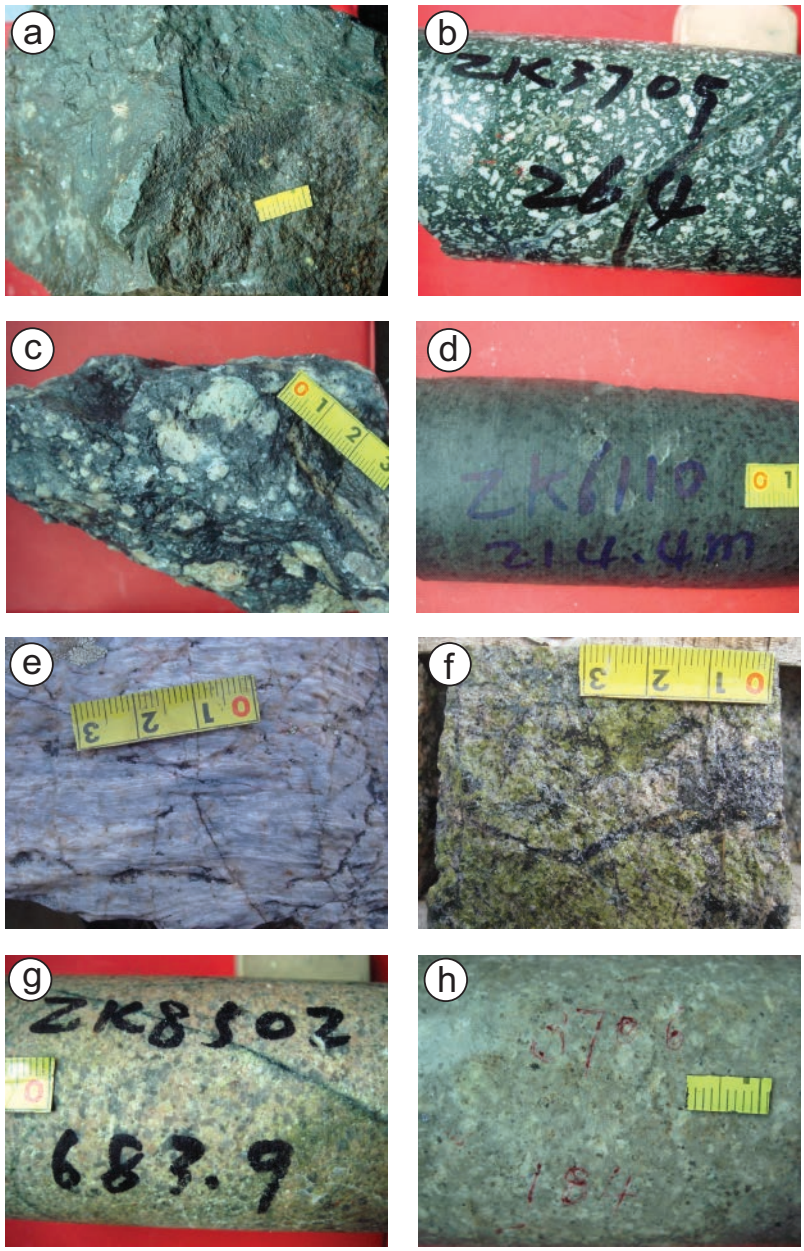

FIG. 4. Photographs of host rocks from the Diyanqinamu deposit: (a). Tuff collected from a trench (TC2103). (b). Volcanic breccia (drill hole ZK3705, depth 264 m). (c). Volcanic breccia collected from surface outcrop. (d). Magnetite-bearing andesite (drill hole ZK6110, 214.4 m). (e). Strongly silicic altered rhyolite from surface outcrop. (f). Propylitic-altered andesite (drill hole ZK2113, 268 m). (g). Phyllic- and propylitic-altered quartz monzonite porphyry (drill hole ZK8502, 683.9 m). (h). Phyllic-altered dacitic porphyry (drill hole ZK3706, 184 m).

%), plagioclase (40 vol %), and minor biotite, quartz, and magnetite.

Hydrothermal alteration

Rocks within the Diyanqinamu deposit record several hydrothermal alteration assemblages, including: propylitic, phyllic, and argillic. Hydrothermal alteration mineral assemblages are presented in detail below and are shown in Figures 4, 5, and 6.

Propylitic alteration is intensely developed in the andesite and volcaniclastic rocks of the Chagannuoer Formation. It is characterized by pervasive disseminations of chlorite, epidote, magnetite, and calcite in these rocks (Figs. 4f, 5d). It also occurs locally in the quartz monzonite porphyry as plagioclase replaced by epidote (Figs. 4g, 6g). During the propylitic alteration, primary mafic minerals (i.e., hornblende and biotite) in these rocks are altered partially or totally to chlorite, whereas plagioclase is altered to epidote and/or calcite. The propylitic alteration zone spatially surrounds the main Mo orebody shown by the projected plan in Figure 7.

Phyllic alteration mainly occurs in tuff and volcanic breccia of the Chagannuoer Formation, quartz monzonite porphyry (Fig. 4g), and dacitic porphyry (Fig. 4h). It overprints the

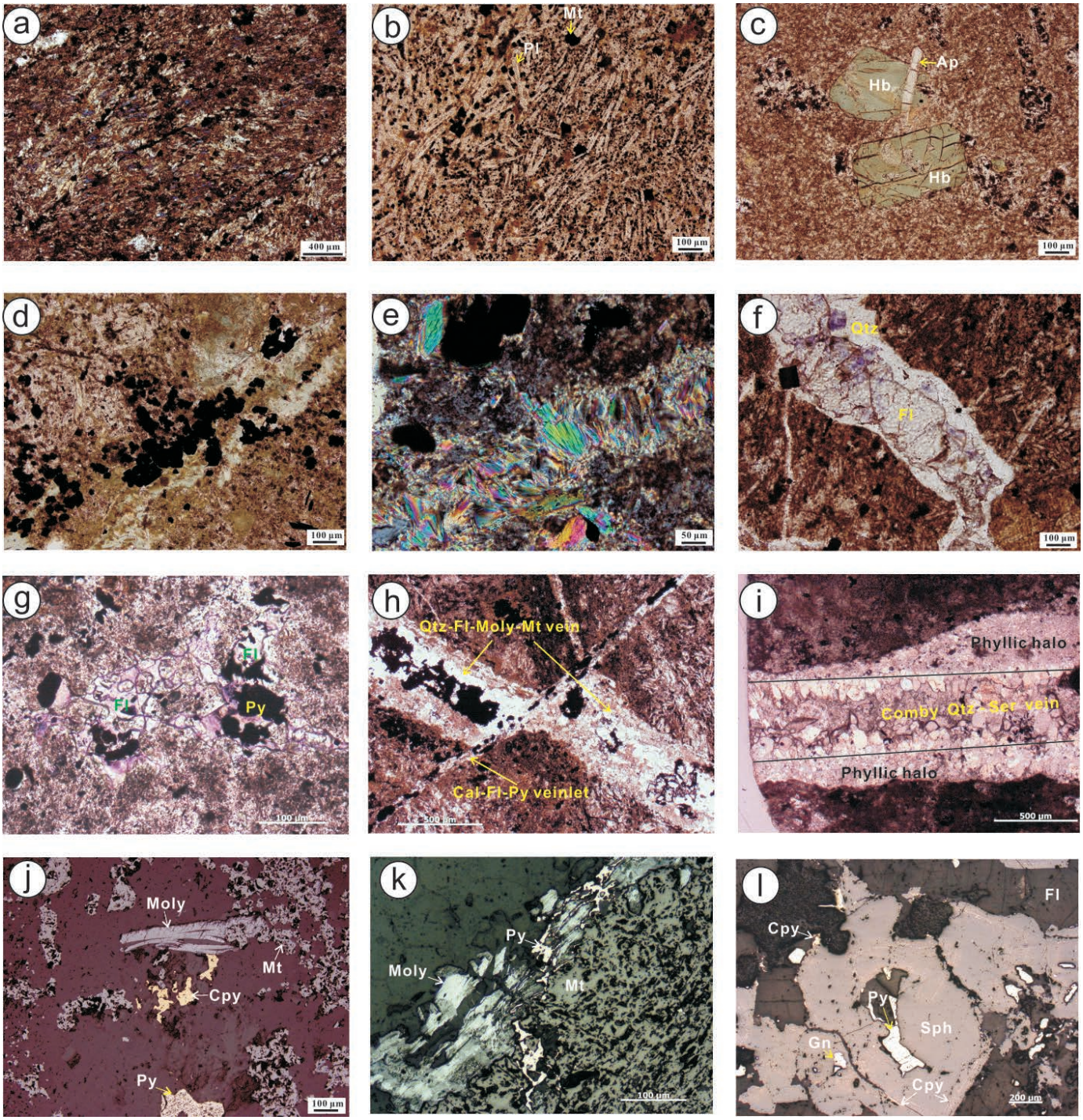

FIG. 5. Microphotographs of some host rocks (a–i) and ores (j–l) from the Diyanqinamu deposit: (a). Tuff with fine-grained tuffaceous texture (drill hole ZK2909, 456 m). (b). Andesite with typical hyalopilitic texture (drill hole ZK6110, 464 m). (c) Andesite with hornblende phenocrysts (drill hole ZK3709, 264 m). (d). Typical propylitic-altered (chlorite-epidote-magnetite assemblage) andesite (drill hole ZK2113, 317.5 m). (e). Phyllic-altered (sericite-quartz-pyrite assemblage) granodiorite porphyry (drill hole ZK8502, 683.9 m). (f). Quartz-fluorite veinlet-bearing volcanic breccia (drill hole ZK5302, 131 m). (g). Disseminated fluorite-bearing phyllic-altered tuff (drill hole ZK6105, 508.3 m). (h). Altered tuff with late calcite-fluorite-pyrite veinlet crosscutting early quartz-fluorite-molybdenite-magnetite vein (drill hole ZK6105, 519 m). (i). Phyllic-altered tuff with irregular strongly phyllic alteration halo in two sides of a comby quartz-sericite vein (drill hole ZK6105, 508.3 m). (j) Molybdenite- chalcopyrite-pyrite-magnetite assemblage in andesite (drill hole ZK7703, 256.3 m). (k). Pyrite veinlets crosscutting magnetite and molybdenite in propylitic altered tuff (drill hole ZK6015, 341.1 m). (l). Sphalerite-pyrite-chalcopyrite-galena coexisting in one fluorite-quartz-calcite vein (drill hole ZK2907, 133 m). Mineral abbreviations: Ap = apatite, Cal = calcite, Cpy = chalcopyrite, Hb = hornblende, Fl = fluorite, Gn = galena, Moly = molybdenite, Mt = magnetite, Qtz = quartz, Pl = plagioclase, Py = pyrite, Ser = sericite, Sph = sphalerite.

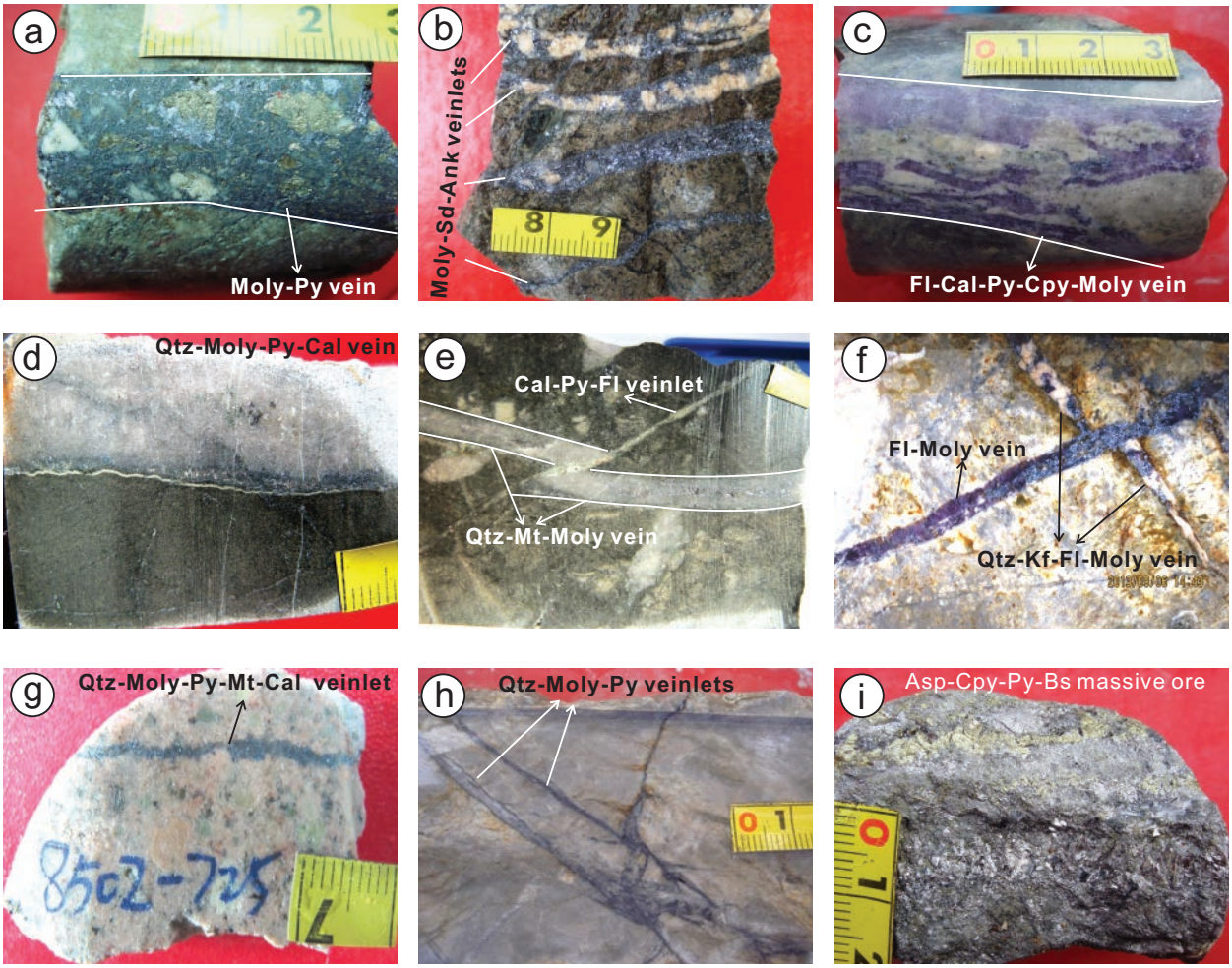

FIG. 6. Photographs of some ore samples from the Diyanqinamu deposit: (a). Molybdenite-pyrite vein in andesite from drill hole ZK3705. (b). Molybdenite-dolomite-siderite veinlets in tuff. (c). Fluorite-calcite-pyrite-chalcopyrite-molybdenite vein in tuff from drill hole ZK3713. (d). Quartz-molybdenite-pyrite -calcite vein in tuff from drill hole ZK6105 at 450.7 m. (e). Late calcite-pyrite-fluorite veinlets crosscutting early quartz-magnetite-molybdenite vein in volcanic breccia from drill hole ZK6105 at 341.1 m. (f). Late fluorite-molybdenite-ankerite vein crosscutting quartz-K-feldspar-fluorite-molybdenite vein. (g). Quartz-molybdenite- pyrite-magnetite-calcite veinlet in the altered quartz monzonite porphyry from drill hole ZK8502 at 724 m. (h). Quartz-molybdenite-pyrite veinlets in silicic-altered tuff from drill hole ZK3705. (i). Massive ore sample consisting of arsenopyrite, chalcopyrite, pyrite, and minor bismuthinite from drill hole ZK2113 at 540 m. Mineral abbreviations: Ank = ankerite, Asp = arsenopyrite, Bs = bismuthinite, Dol = dolomite, Kf = K-feldspar, Sd = siderite. Other abbreviations are the same as in Figure 5.

propylitic alteration zone locally (Fig. 7). It is characterized by pervasive replacement of primary plagioclase by sericite, quartz, illite, and pyrite (Fig. 5e). Some veins and/or veinlets of quartz + muscovite + pyrite + molybdenite with phyllic halos crosscut the quartz monzonite porphyry (Fig. 5e, g, i).

Argillic alteration overprints the propylitic and phyllic alteration zones locally in the southeastern part of the deposit (Fig. 7). Feldspar and sericite in this zone have been replaced by clay minerals including kaolinite, smectite, and illite, which are recognized by near-infrared spectroscopy and XRD analyses (Yan et al., 2012, and our unpub. data). Minor pyrophyllite occurs locally in fractures associated with argillic alteration.

Mineralization and paragenesis

The main Mo orebody occurs in a 2.5-km-long and 2-km-wide volcanic basin (Fig. 3), with the form of a ring about 1,800 m in diameter between lines 17 and 89 in the projected plan (Figs. 3, 7), and looks like a dome in the cross section (Fig. 8). The main Mo orebody is 5 to 450 m thick (avg 82.89 m), and is over 1,000 m in depth. It contains about 0.763 Mt of contained Mo metal resources with an average grade of 0.098% and constitutes approximately 98% of the Mo resource in the deposit. The Mo mineralization occurs unevenly in the propylitic and phyllic altered tuff and andesite. The grade shells of economic mineralization (> 0.06 wt % Mo), low-grade mineralization (0.03 wt % < Mo < 0.06 wt %), and subeconomic rocks (0.015 wt % < Mo < 0.03 wt %) were outlined based on analytical results of drill cores through systematic sampling per meter (Fig. 8).

Based on field and microscopic observations of crosscutting relationships of various veins, and paragenetic relationships of various hydrothermal minerals, five stages of hydrothermal veins have been identified in the deposit (Fig. 9).

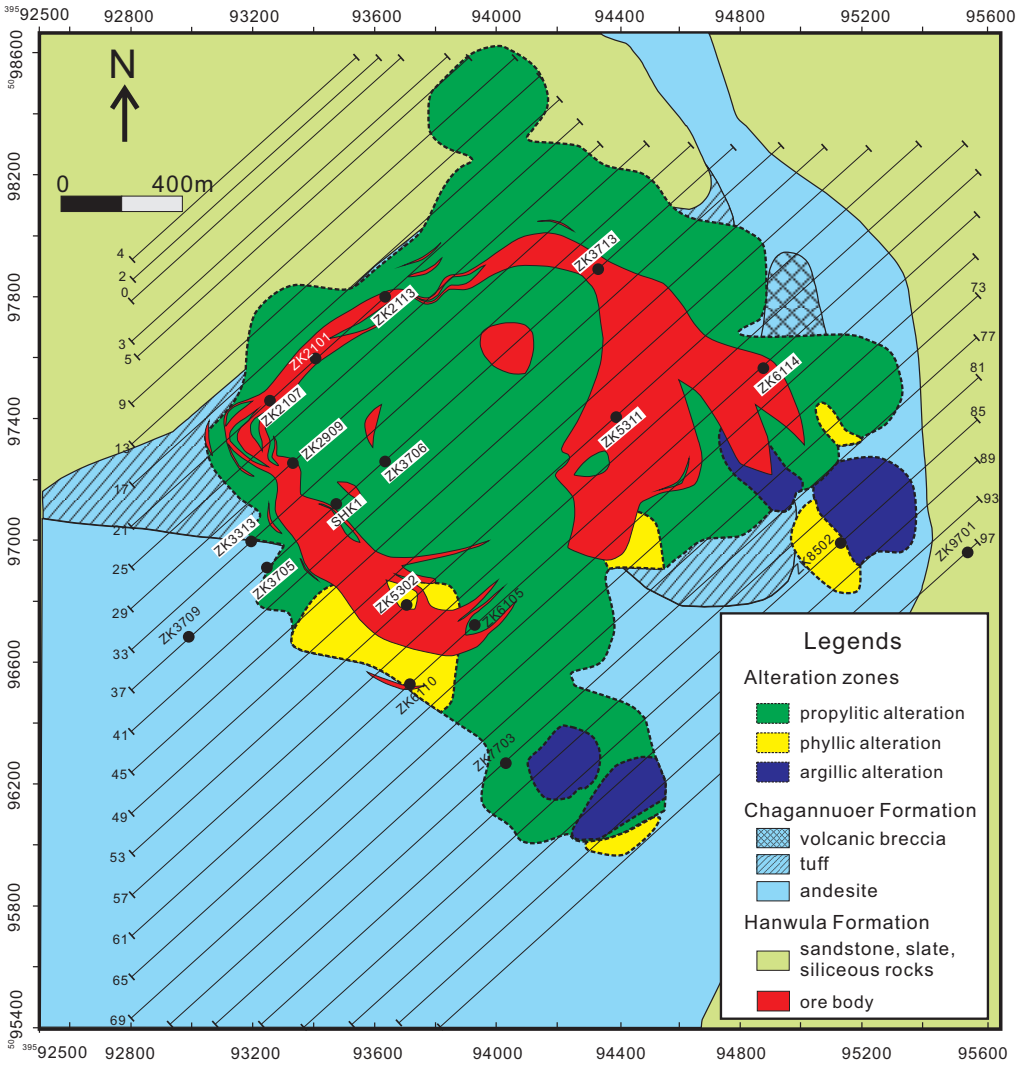

FIG. 7. Hydrothermal alteration zonation at the Diyanqinamu deposit (modified from Yan et al., 2012, and from unpub. data provided by Shandong Gold Group Co. Ltd., 2012).

Stage I: Barren quartz + K-feldspar ± fluorite magnetite ± epidote ± chlorite veinlets are generally less than 2 mm wide, with irregular and discontinuous shape. These veinlets without sharp edges are commonly distributed in the propylitic alteration zone.

Stage II: Quartz + fluorite + molybdenite + magnetite ± pyrite ± sericite ± siderite veinlets/veins commonly occur as 1- to 10-mm-wide veinlets/veins in altered volcanic rocks and the quartz monzonite porphyry, with 1- to 3-mm-wide phyllic alteration halos in most cases (Figs. 5h, i, 6e-h). They have very fine grained magnetite and comby quartz locally (Fig. 5h, i). Molybdenite is interstitial to fine quartz crystals within the veinlets/veins. It is commonly observed that magnetite was locally crosscut by scaly molybdenite (Fig. 5j, k), and both magnetite and molybdenite were crosscut by pyrite veinlets within these veins (Fig. 5k).

Stage III: Fluorite + siderite + quartz + molybdenite + pyrite ± ankerite ± calcite ± chalcopyrite veins are generally 3 to 20 mm wide, with infilling molybdenite commonly intergrown with fluorite in the veins (Fig. 6b, f). These veins are commonly related to phyllic alteration and are accompanied by abundant fluorite occurring in the veins and disseminated in the altered tuff.

Stage IV: Fluorite + quartz + pyrite ± ankerite ± calcite ± molybdenite ± chalcopyrite ± sphalerite ± galena veins are typically 10 to 20 mm wide (Figs. 5l, 6c). These veins are also related to phyllic alteration. In some cases, large amounts of "chalcopyrite disease" are observed under the microscope in brown or light brown sphalerite (Fig. 5l).

Stage V: Narrow (≤5 mm wide) calcite + fluorite + pyrite ± quartz veinlets (Figs. 5h, 6e) occur locally in altered volcanic rocks and typically crosscut the earlier four types of veinlets/veins.

Samples and Analytical Methods

Re-Os molybdenite dating

Ten molybdenite samples collected from different drill holes were chosen for Re-Os isotope dating. The sampling locations, occurrences, and analytical results of these molybdenite samples are given in Table 1.

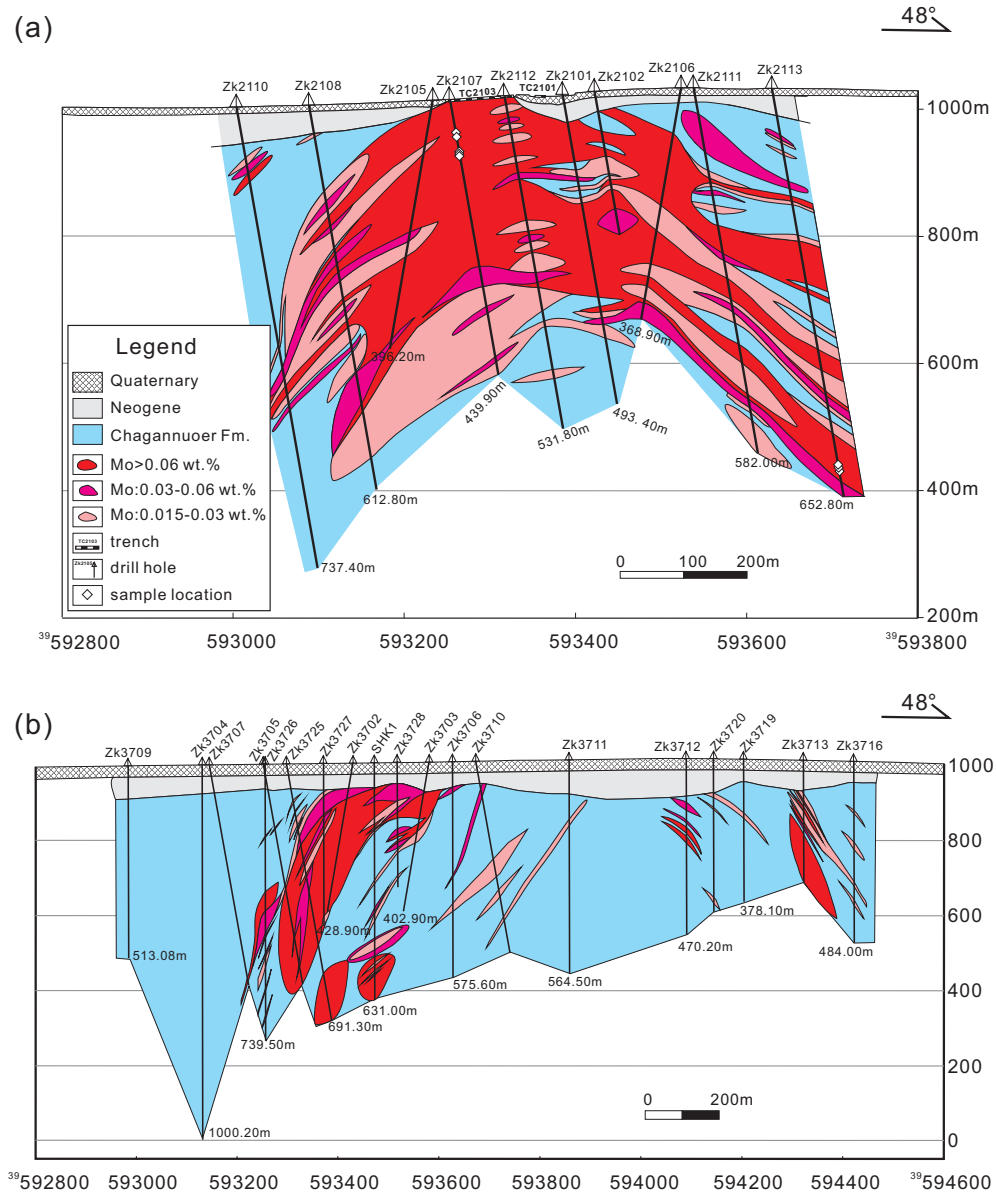

FIG. 8. Geological cross sections along (a) exploration line 21, highlighting the location of molybdenite samples for Re-Os analyses; and (b) exploration line 37 at the Diyanqinamu deposit (modified from unpub. sections provided by Shandong Gold Group Co. Ltd., 2012). The grade shells were outlined based on analytical results of drill cores through systematic sampling per meter.

Molybdenite-bearing veins/veinlets were first cut from their host rocks and crushed to 40 to 80 mesh. Froth flotation (kerosene) was then applied to separate molybdenite from the finely crushed rocks. Molybdenite grains were lastly handpicked under a binocular microscope to get over 99% pure molybdenite separates. Re-Os isotope analyses were performed on a Thermo ICP-MS (TJA X-series) in the Re-Os Laboratory, National Research Center of Geoanalysis, Chinese Academy of Geological Sciences in Beijing. Detailed analytical procedures are described by Du et al. (1994, 2004). A model age of 139.5 ± 2.0 Ma, which is identical to the certified value of 139.6 ± 3.8 Ma (Du et al., 2004), for the molybdenite standard GBW04436 was obtained during our analytical session. Blanks are 2.9 ± 0.9 pg for Re and 0.1 pg for Os. An ^{187}Re decay constant of 1.666×10^{-11} year^{-1} (Smoliar et al., 1996) has been used to calculate the molybdenite model ages. An Re-Os isochron age was calculated by using the ISOPLOT 2.49 program (Ludwig, 2001). Uncertainty in Re-Os model age calculations include (1) 1.02% uncertainty in the ^{187}Re decay constant, (2) weighing uncertainty for both spike and sample, (3) uncertainty in spike calibration, and (4) mass spectrometry analytical uncertainty.

Sulfur and lead isotope analyses

Forty-three sulfide samples including molybdenite, pyrite, chalcopyrite, sphalerite, and galena were selected from different parts of orebodies for sulfur isotope analyses. Sulfide-bearing veins/veinlets were first cut from their host rocks and

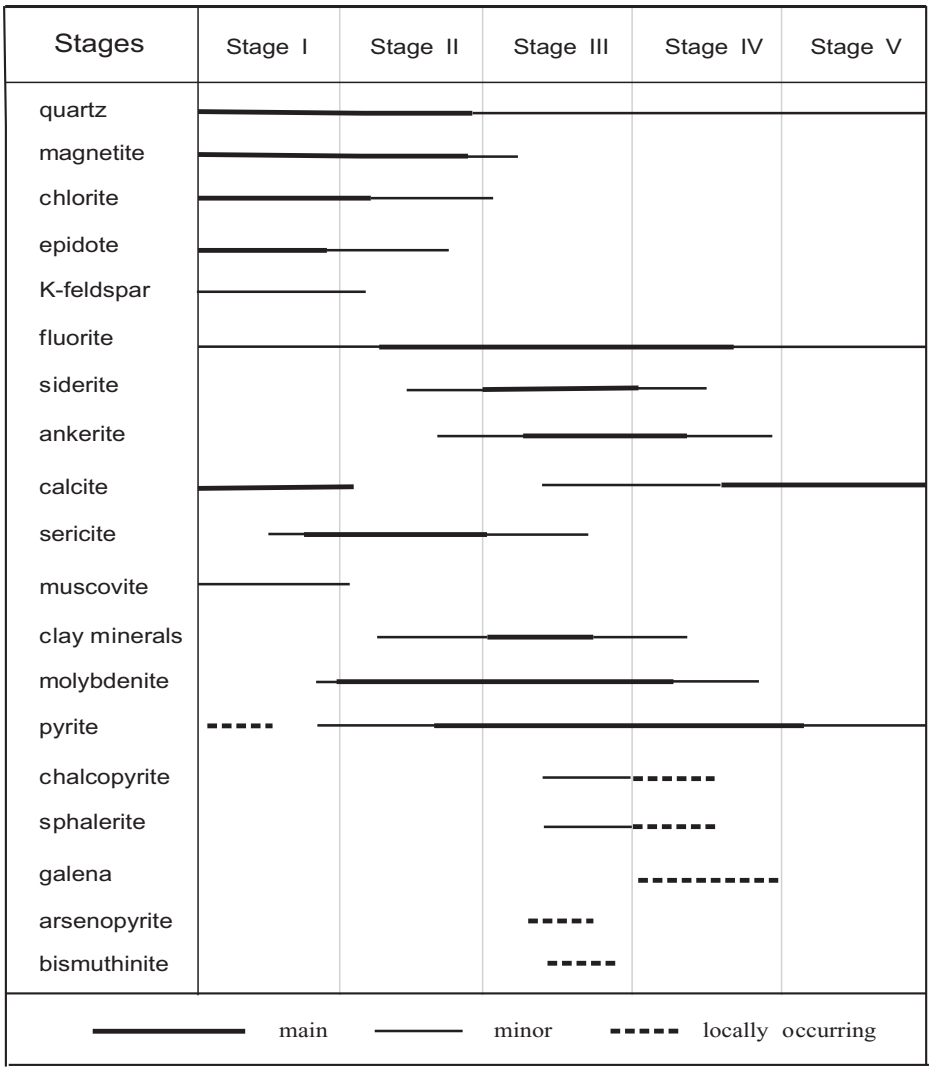

FIG. 9. Simplified paragenetic sequence of ore and gangue minerals from the Diyanqinamu deposit.

crushed to 40 to 80 mesh; sulfide minerals were then hand-picked under a binocular microscope to remove impurities. Sulfide separates were then crushed to <200-mesh powder in an agate mortar. Sulfur isotope analyses were completed using a Finnigan MAT-252 mass spectrometer according to the method of Ueda and Sakai (1984) at the State Key Laboratory of Environmental Geochemistry, Chinese Academy of Sciences in Guiyang. The sulfide powder was enclosed in a tin cup and then put into a reacting furnace. Subsequently, the powder was oxidized to $SO_{2(g)}$. Helium was used as a carrier gas and mixed with SO_2 to facilitate transport into the mass spectrometer. Reference standards GBW04414 and GBW04415 were used as external standards to calibrate the sulfur isotope composition of unknown samples. During our analytical session, the obtained $\delta^{34}S$ values are –0.10 ± 0.17‰ (2σ; n = 12) for standard GBW04414, consistent with its recommended value of –0.07 ± 0.13‰ (2σ; Ding et al., 2001). The analytical precision is typically ±0.2‰ (2σ).

Lead isotope compositions of sulfides were analyzed on an IsoProbe-T thermal ionization mass spectrometer (TIMS) at the Analytical Laboratory of the Beijing Research Institute of Uranium Geology. Lead was separated and purified by a conventional cation-exchange technique (AG1 × 8, 200–400 resin) with diluted HBr used as eluant. The $^{208}Pb/^{206}Pb$, $^{207}Pb/^{206}Pb$, and $^{204}Pb/^{206}Pb$ ratios of the Standard NBS 981 were 2.16810 ± 0.0008 (2σ), 0.91464 ± 0.00033 (2σ), and 0.059042 ± 0.000037 (2σ), respectively. They are consistent with their corresponding recommended values of 2.16701 ± 0.00013 (2σ), 0.91459 ± 0.00009 (2σ), and 0.059047 ± 0.000024 (2σ; Todt et al., 1996).

Results

Re-Os molybdenite ages

Total Re concentrations of ten molybdenite samples vary from 19.6 to 89.1 ppm (Table 1). Eight molybdenite samples from veins/veinlets of two mineral assemblages in drill cores of ZK2107 and ZK2113 have similar Re from 42.6 to 58.2 ppm, whereas the other two samples (ZK3713-248 and ZK6105-285) respective from drill core of ZK3713 and ZK6105 have 19.6 and 89.1 ppm Re, respectively (Table 1). Re-Os molybdenite model ages range from 157.6 ± 2.4 to

Table 1. Re-Os Data for Molybdenites from the Diyanqinamu Porphyry Mo Deposit, Inner Mongolia

Sample no.	Sampling location: Drill hole	Depth (m)	Vein stages	Occurrence	Weight (g)	Re (ppm): Measured	±2σ	Common Os (ppb): Measured	±2σ	^{187}Re (ppm): Measured	±2σ	^{187}Os (ppb): Measured	±2σ	Model age (Ma): Measured	±2σ
ZK2107-85.4	ZK2107	85.4		Two 2- to 8-mm-wide quartz-fluorite-molybdenite veins in propylitic-altered volcanic breccia	0.05021	42.58	0.36	0.0098	0.0330	26.76	0.23	70.07	0.56	157.0	2.2
ZK2107-91.7	ZK2107	91.7	II	One 10-mm-wide quartz-molybdenite vein in propylitic-altered tuff	0.03024	52.94	0.42	0.0122	0.0546	33.27	0.26	86.14	0.75	155.2	2.2
ZK2107-93.5	ZK2107	93.5	II	One 5-mm-wide quartz-fluorite-molybdenite-magnetite veinlet in the propylitic-altered tuff	0.03040	50.94	0.52	0.0119	0.0400	32.02	0.33	82.80	0.76	155.0	2.5
ZK3713-248	ZK3713	248	II	One 10-mm-wide quartz-molybdenite vein in phyllic-altered volcanic breccia	0.05021	19.59	0.17	0.0098	0.0110	12.31	0.11	32.06	0.26	156.1	2.3
ZK6105-285	ZK6105	285	II	One 8-mm quartz-molybdenite vein in silicic-altered volcanic tuff	0.03045	89.13	0.76	0.0094	0.0316	56.02	0.48	146.87	1.21	157.2	2.3
ZK2113-606	ZK2113	606	III	One 30-mm-wide fluorite-siderite-ankerite-quartz-molybdenite-pyrite vein in phyllic-altered volcanic tuff	0.05039	58.15	0.57	0.0098	0.0220	36.55	0.36	95.08	0.83	155.9	2.4
ZK2107-58.5	ZK2107	58.5	III	One 20-mm-wide molybdenite-pyrite-quartz vein in phyllic-altered volcanic tuff	0.03005	50.19	0.43	0.0132	0.0295	31.55	0.27	81.94	0.71	155.7	2.3
ZK2107-58.9	ZK2107	58.9	III	One 18-mm-wide molybdenite-pyrite-quartz vein in phyllic-altered volcanic tuff	0.03010	50.85	0.41	0.0121	0.0270	31.96	0.26	82.78	0.66	155.3	2.2
ZK2113-607.5	ZK2113	607.5	III	Two 3- to 15-mm-wide siderite-ankerite-fluorite-molybdenite-pyrite veins phyllic-altered volcanic tuff	0.03062	54.98	0.49	0.0119	0.0534	34.55	0.31	90.24	0.85	156.6	2.4
ZK2113-609.3	ZK2113	609.3	III	One 15-mm-wide quartz-ankerite-molybdenite vein in phyllic-altered quartz monzonite porphyry	0.03023	45.54	0.42	0.0120	0.0269	28.62	0.27	75.25	0.67	157.6	2.4

155.0 ± 2.5 Ma and show an excellent reproducibility. All the analyses yield an average Re-Os model age of 156.2 ± 0.7 Ma (2σ, MSWD = 0.60, n = 10; Fig. 10a) and an ^{187}Re-^{187}Os isochron age of 156.2 ± 1.4 Ma (2σ, MSWD = 0.96, n = 10; Fig. 10b). But these high internal precisions (0.4–0.9%) of Re-Os data should be expanded up to ~2.7% as an external precision, if the propagation of the uncertainties from the standard (GBW04436, 139.6 ± 3.8 Ma) is considered adequately. This means that the age of 156.2 ± 4.2 Ma best represents the age of molybdenite mineralization at Diyanqinamu and is used to compare with other ages obtained from different geochronometers (i.e., zircon U-Pb).

Sulfur isotope compositions of sulfide minerals

The $\delta^{34}S$ values of sulfides are listed in Table 2 and range from 2.5 to 10.2‰ with an average value of 7.2 ± 2.2‰ (n = 43), significantly higher than those of mantle (0 ± 3‰, Chaussidon et al., 1989) and most porphyry systems (0 ± 5‰, Ohomoto and Rye, 1979), suggesting that a ^{34}S-enriched sulfur source contributed to at least part of the Diyanqinamu sulfur inventory. Twenty-one molybdenite samples record a broad range of $\delta^{34}S$ values varying from 3.3 to 10.2‰ (mean = 8.2 ± 2.4‰, with 15 out of 21 values higher than the mean of 8.2‰), whereas the ranges of $\delta^{34}S$ values for other sulfides are more restricted, i.e., 5.2 to 8.3‰ (n = 15, mean = 6.8 ± 1.1‰) for pyrite, 5.8 to 6.7‰ (n = 3, mean = 6.2 ± 0.4‰) for sphalerite, 6.1 to 6.7‰ (n = 2, mean = 6.4 ± 0.4‰) for chalcopyrite, and 2.5 to 3.4‰ (n = 2, mean = 3.0 ± 0.7‰) for galena. When plotted by vein paragenesis, it can be seen in Figure 11 that $\delta^{34}S_{pyrite}$ values roughly decrease from the earlier to the later stages.

Lead isotope compositions of sulfide minerals

Pb isotope compositions of sulfide separates are listed in Table 3 and plotted in Figure 12. The Pb isotope values presented here are present-day values, which in most case reflect "initial" isotope values at the time of deposition, because most sulfides (i.e., pyrite, galena, and molybdenite) generally have low U and Th contents. Overall, the $^{207}Pb/^{204}Pb$ ratios

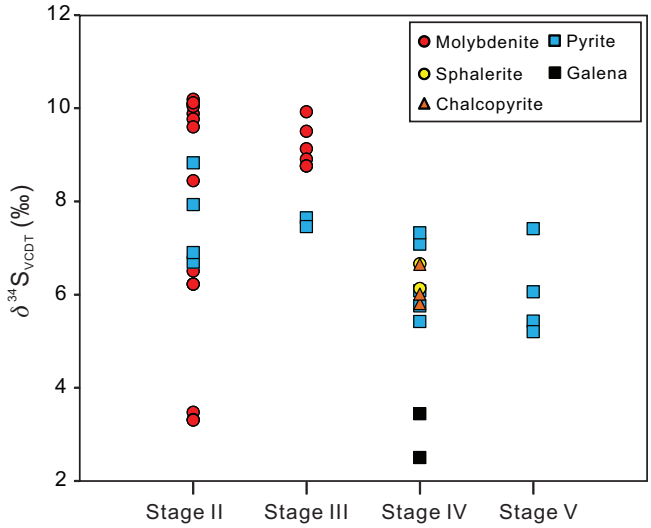

FIG. 11. $\delta^{34}S$ values of various sulfides from different vein stages in the Diyanqinamu deposit. The sulfur isotope values are listed in Table 2. See text for explanation.

display positive correlations with the ratios of $^{208}Pb/^{204}Pb$ and $^{206}Pb/^{204}Pb$ (Fig. 12a, b), suggesting a mixing trend of two or more isotopically distinct sources. Moreover, compared with other sulfide minerals (including galena, pyrite, sphalerite, and chalcopyrite), molybdenite generally has relatively lower $^{206}Pb/^{204}Pb$, $^{207}Pb/^{204}Pb$, and $^{208}Pb/^{204}Pb$ ratios that range from 18.266 to 18.361, 15.493 to 15.552, and 37.909 to 38.085, respectively, although the data ranges overlap (Fig. 12; Table 3).

Discussion

Timing of mineralization

Previous studies have shown that the Late Permian-Triassic (235–224 Ma) and Early Cretaceous (137–131 Ma) periods are important epochs of porphyry Mo-(W-Cu) mineralization in the Chagan Obo-Aoyoute-Chaobulen tectono-magmatic

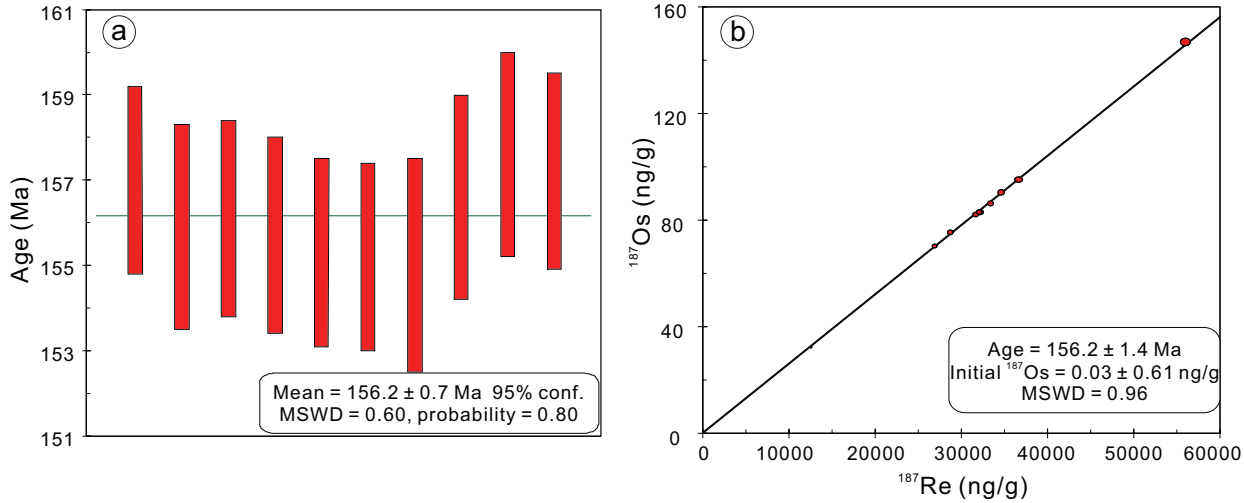

FIG. 10. (a). Re-Os weighted average model age diagram. (b). Isochron diagram for molybdenite samples from the Diyanqinamu deposit. The Re-Os ages are listed in Table 1.

TABLE 2. Sulfur Isotope Compositions ($\delta^{34}S_{VCDT}$) of the Sulfides from the Diyanqinamu Porphyry Mo Deposit, Inner Mongolia

	Sampling location			$\delta^{34}S$ (‰)				
Sample no.	Drill hole	Depth (m)	Vein stages	Moly	Py	Cpy	Sph	Gn
ZK2107-85.4	ZK2107	85.4	II	10.0				
ZK2107-91.7	ZK2107	91.7		9.9				
ZK2107-93.5	ZK2107	93.5		9.8				
ZK2111-159.5	ZK2111	159.5			8.8			
ZK2113-177.4	ZK2113	177.4			6.7			
ZK3117-197	ZK3117	197		10.1				
ZK3713-213.5	ZK3713	213.5		10.2				
ZK3713-239	ZK3713	239			6.9			
ZK3713-248	ZK3713	248		9.6	7.9			
ZK3713-278	ZK3713	278		10.0				
ZK3713-281.7	ZK3713	281.7		10.1				
ZK6105-184.8	ZK6105	184.8		8.4				
ZK6105-285	ZK6105	285		6.2				
ZK6105-286b	ZK6105	286		6.2				
ZK6105-399.1	ZK6105	399.1		3.5				
ZK6105-399.5a	ZK6105	399.5		3.3				
ZK6105-399.5b	ZK6105	399.5		3.3				
ZK8502-298	ZK8502	298		6.5				
ZK2107-58.5	ZK2107	58.5	III	9.5				
ZK2107-58.9	ZK2107	58.9		9.9	7.7			
ZK2113-601	ZK2113	601		9.1				
ZK2113-606	ZK2113	606		8.9				
ZK2113-609.3	ZK2113	609.3		8.8				
ZK3705-405	ZK3705	405		8.8	7.5			
ZK2907-132.6	ZK2907	132.6	IV				6.7	
ZK2907-134	ZK2907	134					5.8	3.4
ZK3705-192.3	ZK3705	192.3			5.4			
ZK3705-221.5	ZK3705	221.5			5.8		6.0	
ZK3705-250	ZK3705	250			7.1	6.1		
ZK3705-255.6	ZK3705	255.6			6.1			
ZK3705-556	ZK3705	556			7.3	6.7		
ZK5113-154.3	ZK5113	154.3						2.5
ZK3705-266	ZK3705	266	V		6.1			
ZK3713-249	ZK3713	249			7.4			
ZK8502-509.3	ZK8502	509.3			5.4			
ZK8502-515.3	ZK8502	515.3			5.2			

Mineral abbreviations: Cpy = chalcopyrite, Gn = galena, Moly = molybdenite, Py = pyrite, Sph = sphalerite

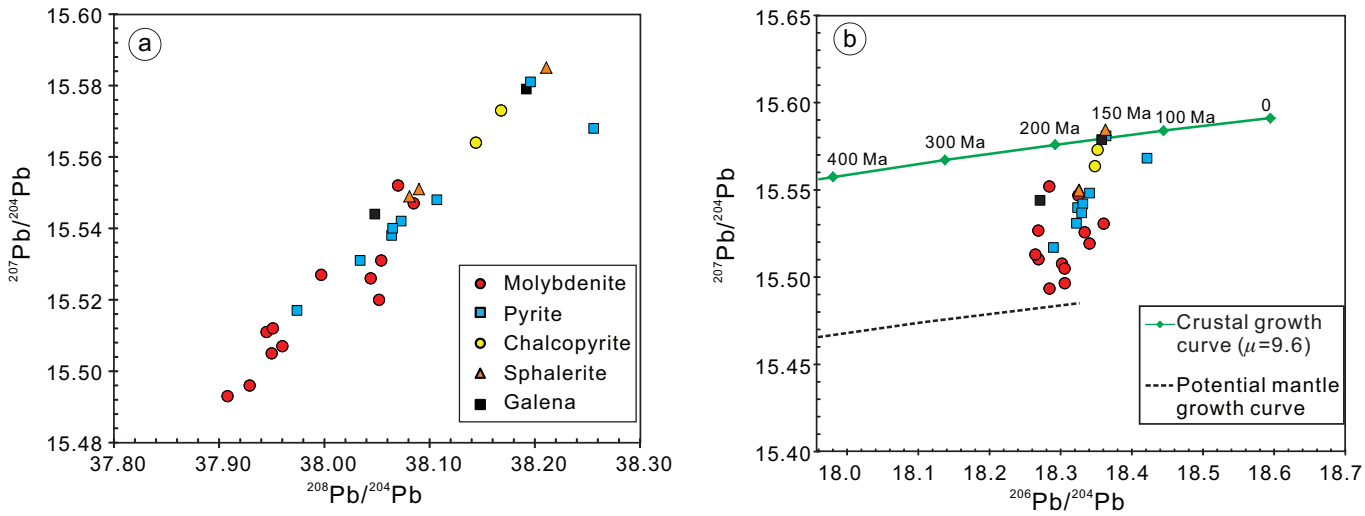

FIG. 12. (a). $^{208}Pb/^{204}Pb$ versus $^{207}Pb/^{204}Pb$ diagram. (b). Two-stage Pb isotope evolution diagram for sulfides from the Diyanqinamu deposit. The symbol size is larger than the analytical uncertainties. All Pb isotope data are provided in Table 3. See text for explanation.

Table 3. Pb Isotope Composition of Sulfide Minerals from the Diyanqinamu Porphyry Mo Deposit, Inner Mongolia

Sample no.	Sampling location		Vein stages	Analyzed mineral	$^{208}Pb/^{204}Pb$	$\pm2\sigma$	$^{207}Pb/^{204}Pb$	$\pm2\sigma$	$^{206}Pb/^{204}Pb$	$\pm2\sigma$
	Drill hole	Depth (m)								
ZK3713-248	ZK3713	248	II	Molybdenite	38.054	0.005	15.531	0.002	18.361	0.002
ZK2107-85.4	ZK2107	85.4		Molybdenite	37.95	0.005	15.505	0.002	18.306	0.002
ZK2107-91.7	ZK2107	91.7		Molybdenite	37.908	0.006	15.493	0.003	18.285	0.003
ZK2107-93.5	ZK2107	93.5		Molybdenite	37.96	0.003	15.507	0.001	18.303	0.002
ZK6105-285	ZK6105	285		Molybdenite	37.997	0.004	15.527	0.002	18.269	0.002
ZK3713-278	ZK3713	278		Molybdenite	38.052	0.004	15.52	0.001	18.34	0.002
ZK6105-399.5	ZK6105	399.5		Molybdenite	38.044	0.004	15.526	0.001	18.334	0.002
ZK3713-213.5	ZK3713	213.5		Molybdenite	38.085	0.004	15.547	0.001	18.326	0.001
ZK3713-248	ZK3713	248		Pyrite	38.034	0.003	15.531	0.001	18.322	0.002
ZK3713-239	ZK3713	239		Pyrite	38.073	0.004	15.542	0.002	18.33	0.002
ZK2113-177.4	ZK2113	177.4		Pyrite	38.256	0.004	15.568	0.002	18.421	0.002
ZK2113-606	ZK2113	606	III	Molybdenite	38.07	0.006	15.552	0.003	18.285	0.003
ZK2107-58.9	ZK2107	58.9		Molybdenite	37.945	0.003	15.511	0.001	18.268	0.002
ZK2113-609.3	ZK2113	609.3		Molybdenite	37.951	0.004	15.512	0.002	18.266	0.002
ZK2107-58.5	ZK2107	58.5		Molybdenite	37.929	0.003	15.496	0.001	18.307	0.002
ZK3705-405	ZK3705	405		Pyrite	38.196	0.004	15.581	0.002	18.363	0.002
ZK3705-556	ZK3705	556	IV	Chalcopyrite	38.168	0.003	15.573	0.001	18.352	0.002
ZK3705-250	ZK3705	250		Chalcopyrite	38.144	0.004	15.564	0.002	18.348	0.002
ZK3713-154.3	ZK3713	154.3		Galena	38.048	0.004	15.544	0.002	18.272	0.002
ZK2907-134	ZK2907	134		Galena	38.192	0.005	15.579	0.002	18.358	0.003
ZK3705-192.3	ZK3705	192.3		Pyrite	38.107	0.003	15.548	0.001	18.341	0.002
ZK3705-250	ZK3705	250		Pyrite	38.064	0.004	15.538	0.001	18.329	0.002
ZK3705-221.5	ZK3705	221.5		Pyrite	38.065	0.004	15.54	0.002	18.324	0.002
ZK2907-134	ZK2907	134		Sphalerite	38.211	0.004	15.585	0.002	18.363	0.002
ZK2907-132.6	ZK2907	132.6		Sphalerite	38.081	0.006	15.549	0.003	18.323	0.003
ZK3705-221.5	ZK3705	221.5		Sphalerite	38.09	0.006	15.551	0.002	18.326	0.002
ZK8502-509.3	ZK8502	509.3	V	Pyrite	37.974	0.004	15.517	0.002	18.29	0.002

belt (Nie and Jiang, 2011). However, here we show that the Diyanqinamu porphyry Mo deposit has a molybdenite Re-Os age of 156.2 ± 4.2 Ma, which is consistent with zircon U-Pb ages of porphyry intrusions in the deposit (156 ± 2 Ma, Sun et al., 2014) within errors. These ages are slightly younger that the eruptive ages of the andesitic host rocks (165 ± 3 Ma, Shandong Gold Group Co. Ltd., unpub. data, 2012). It thus seems that Mo mineralization at Diyanqinamu was associated with emplacement of the porphyries, although the specific causative intrusions have not been identified yet.

Porphyry Mo-(Cu) deposits with ages varying from 170 to 150 Ma have been widely reported in the Russian Far East (e.g., the Zhireken and Shakhtama porphyry Mo-Cu deposits, Fig. 1; Sotnikov et al., 2001; Berzina et al., 2005, 2013), and in the Xilamulun tectonic-metallogenic belt along the northern margin of the North China craton, e.g., the Jiguanshan porphyry Mo deposit (Fig. 1; Zhang et al., 2009; Wu et al., 2011). Furthermore, Au-Ag deposits associated with Late Jurassic granitoid intrusions (165–146 Ma) are also known on both sides of the Mongol-Okhotsk suture (e.g., Koval et al., 1999; Zorin et al., 2001). We therefore suggest that the Late Jurassic could be a third significant epoch for porphyry Mo-(Cu-W) mineralization in Inner Mongolia.

Possible sources of sulfur and metals

In general, $\delta^{34}S_{sulfide}$ values for most porphyry-type deposits in the world range from –5 to 5‰ (Fig. 13), which are roughly consistent with the accepted mantle range (0 ± 3‰; Chaussidon et al., 1989). However, a few porphyry deposits, such as the Sams Creek porphyry Au deposit from New Zealand ($\delta^{34}S_{sulfide}$ values varying from 4.9–9.9‰ with a mean of 8.1‰, Faure and Brathwaite, 2006), and the Sora (from 6.6–10.2‰ with a mean of 8.5‰) and Shakhtama (from 2.9–8.4‰ with a mean of 6.0‰) porphyry Mo deposits from Siberia (Sotnikov et al., 2004) show $\delta^{34}S_{sulfide}$ values higher than 5‰. Our results show that most of the sulfides from Diyanqinamu have $\delta^{34}S$ values higher than 5.0‰ (Figs. 11, 13), and molybdenite and pyrite from early stages in the paragenesis (i.e., Stages II and III) generally have higher $\delta^{34}S$ values than those of pyrite, chalcopyrite, galena, and sphalerite from later stages (Fig. 11). These relatively high $\delta^{34}S$ values could either be inherited from the magmatic source, or result from contamination by crustal marine sedimentary facies or evaporites with high $\delta^{34}S$ values (e.g., Faure and Brathwaite, 2006). Due to the fact that no marine evaporites or carbonates have been reported near the Diyanqinamu deposit (although some Late Permian to Early Triassic fossiliferous marine sedimentary rocks occur in eastern Mongolia; Kovalenko et al., 1995), and that the mantle in this region has generally high $\delta^{34}S$ values (5–7‰; Ionov et al., 1992), we therefore suggest that the relatively high $\delta^{34}S$ values of the sulfides from Diyanqinamu could be inherited from the magmatic source.

Lead isotope compositions of molybdenite, pyrite, chalcopyrite, sphalerite, and galena are interpreted to be the "initial" ratios present in the source of ore-bearing fluids at various stages of mineralization. A two-stage model of Stacey and Kramers (1975) is adopted in this study, with a second stage μ value ($^{238}U/^{204}Pb$ ratio) of 9.6. This value is chosen to allow three analyses (sphalerite, galena, and pyrite, one of each) of the highest $^{207}Pb/^{204}Pb$ ratios (~15.58) to be plotted on the growth curve at ~155 Ma in the $^{207}Pb/^{204}Pb$ versus $^{206}Pb/^{204}Pb$ diagram (Fig. 12b). The data form an elongate narrow trend

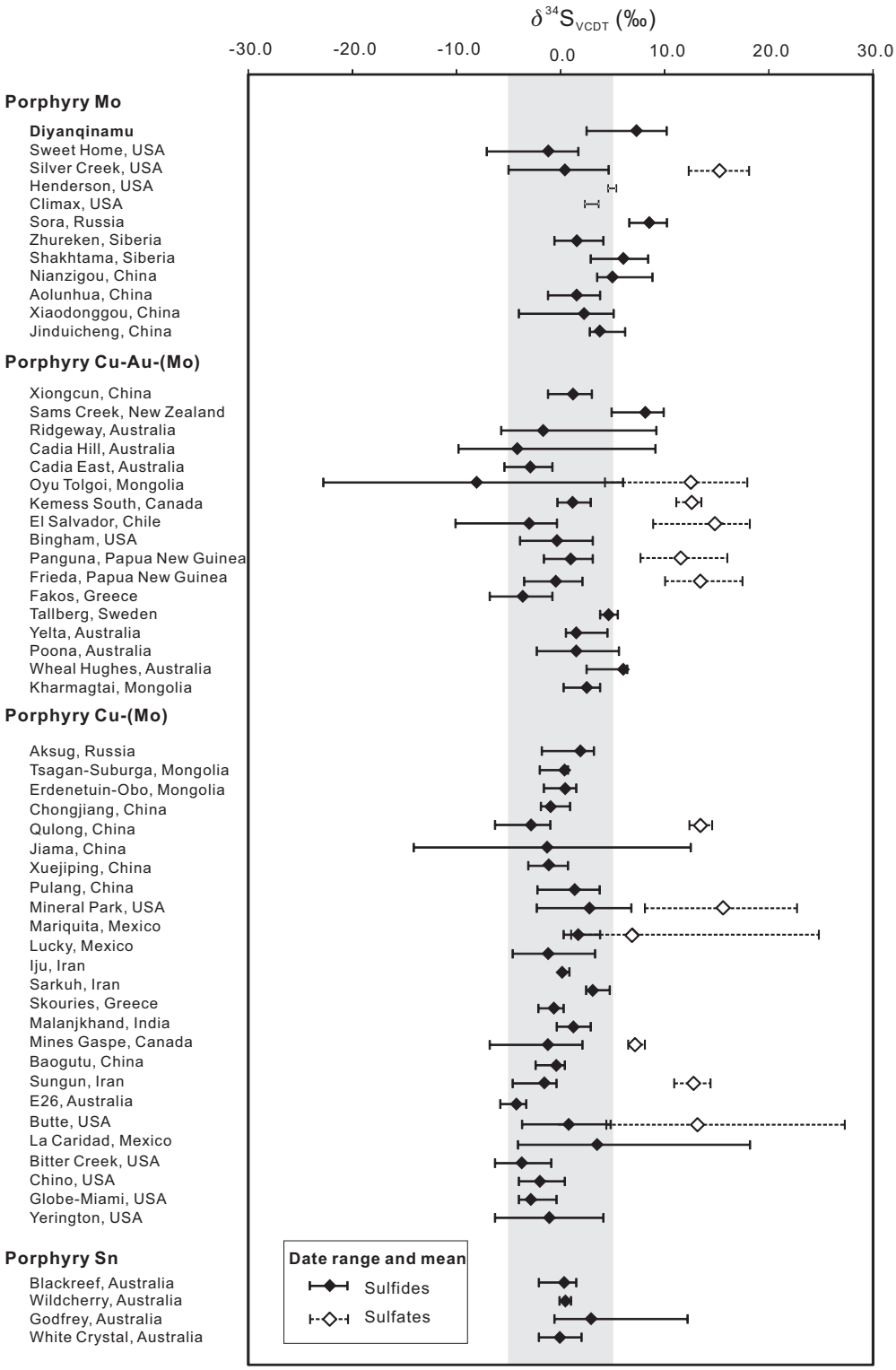

FIG. 13. A compilation of sulfur isotope compositions for sulfide and sulfate minerals from porphyry-type deposits around the world. Data for the Diyanqinamu deposit are from this study. Other data are from Field (1966), Field and Gustafson (1976), Ohomoto and Rye (1979), Shelton and Rye (1982), Eastoe (1983), Stein and Hannah (1985), Lang et al. (1989), Frei (1995), Ren et al. (1995), Sarkar et al. (1996), Wareham et al. (1998), Watanabe and Hedenquist (2001), Morales Ruano et al. (2002), Calagari (2004), Sotnikov et al. (2004), Field et al. (2005), Faure and Brathwaite (2006), Meng et al. (2006), Qu et al. (2007), Wang et al. (2007), Wilson et al. (2007), Valencia et al. (2008), Duuring et al. (2009), Lüders et al. (2009), Li et al. (2010, 2014), Liu and Zhou (2010), Shen et al. (2012), Del Rio Salas et al. (2013), Mirnejad et al. (2013), Ying et al. (2013), and references therein. For the Henderson and Climax porphyry Mo deposits, only a variation range of $\delta^{34}S_{sulfides}$ values was provided by Stein and Hannah (1985).

that transects the defined growth curves, with molybdenite showing relatively lower $^{208}Pb/^{204}Pb$ and $^{207}Pb/^{204}Pb$ ratios than those of other sulfides, especially chalcopyrite, galena, and sphalerite. A likely interpretation for the variation of Pb isotope signatures is that a mixing of two or more isotopically distinct sources was involved in the ore-forming process. In this case, mixing a low $^{208}Pb/^{204}Pb$ and $^{207}Pb/^{204}Pb$ magmatic fluid (probably from the underlying porphyries) with isotopically evolved crustal materials is a plausible explanation. As mentioned above, molybdenite that formed in Stages II and III shows relatively high $\delta^{34}S$ values, whereas chalcopyrite, sphalerite, and galena from later Stages III and IV have relatively low $\delta^{34}S$ values, and pyrite that formed throughout the paragenesis shows decreasing $\delta^{34}S$ values. In combination with the Pb isotope signatures, it is therefore speculated that molybdenum was sourced from magmatic fluids at the Diyanqinamu deposit. In contrast, chalcopyrite, sphalerite, and galena, which were precipitated later in the paragenesis, display a greater crustal signature, suggesting that they were precipitated from fluids that had been diluted by fluids carrying Pb and S of crustal origin. Pyrite, which forms throughout the paragenesis, shows a range of Pb isotope compositions between those of the molybdenite in earlier stages and the other sulfides in later stages, reflecting this transition in S sources.

Conclusions

The Diyanqinamu porphyry Mo deposit in the southern Greater Khingan Range of Inner Mongolia is hosted in Late Jurassic volcanic rocks. Five stages of mineralization are associated with propylitic and phyllic alterations. Molybdenite mainly occurs in veins and veinlets that contain quartz, fluorite, magnetite, and pyrite, with minor ankerite, siderite, chalcopyrite, sphalerite, and galena, and is associated with phyllic alteration. Re-Os molybdenite dating results indicate that this deposit formed at ~156 Ma and it was probably related to the Late Jurassic felsic magmatism in this area. Sulfur and lead isotope data for sulfide minerals, together with their paragenesis, suggest a mantle-like, magmatic signature for the early vein stages (including molybdenite), whereas later vein stages (containing galena, sphalerite, and chalcopyrite) have a greater crustal signature. This could reflect dilution of an early magmatic fluid by fluids carrying Pb and S of crustal origin.

Acknowledgments

This manuscript has greatly benefited from patient and constructive reviews by Jeremy Richards, David Sinclair, and Christopher Lawley. Many thanks are due to Andao Du, Wenjun, Qu, Ning An, and Jianyong Cui for their assistance in isotope analyses. We highly appreciate David Cooke, Meifu Zhou, Xinfu Zhao, Wei Chen, and Pingping Liu for their helpful suggestions and language improvement on drafts of this manuscript. We also appreciate the Shandong Gold Group Co., Ltd. for funding this project. This study was also supported by grants from 973 (2013CB429801) and the Natural Science Foundation of China (41373051).

REFERENCES

Berzina, A.N., Sotnikov, V.I., Economou-Eliopoulos, M., and Eliopoulos, D.G., 2005, Distribution of rhenium in molybdenite from porphyry Cu-Mo and Mo-Cu deposits of Russia (Siberia) and Mongolia: Ore Geology Reviews, v. 26, p. 91–113.

Berzina, A.P., Berzina, A.N., Gimon, V.O., Krymskii, R.S., Larionov, A.N., Nikolaeva, I.V., and Serov, P.A., 2013, The Shakhtama porphyry Mo ore-magmatic system (eastern Transbaikalia): Age, sources, and genetic features: Russian Geology and Geophysics, v. 54, p. 587–605.

Calagari, A.A., 2004, Fluid inclusion studies in quartz veinlets in the porphyry copper deposit at Sungun, East-Azarbaidjan, Iran: Journal of Asian Earth Sciences, v. 23, p. 179–189.

Chaussidon, M., Albarede, F., and Sheppard, S.M.F., 1989, Sulphur isotope variations in the mantle from ion microprobe analyses of micro-sulphide inclusions: Earth and Planetary Science Letters, v. 92, p. 144–156.

Chen, Z.G., Zhang, L.C., Wu, H.Y., Wan, B., and Zeng, Q.D., 2008, Geochemistry study and tectonic background of a style host granite in Nianzigou molybdenum deposit in Xilamulun molybdenum metallogenic belt, Inner Mongolia: Acta Petrologica Sinica, v. 24, p. 879–898 (in Chinese with English abs.).

Del Rio Salas, R., Ochoa-Landín, L., Ruiz, J., Eastoe, C., Meza-Figueroa, D., Zuniga-Hernandez, H., Mendívil-Quijada, H., and Quintanar-Ruiz, F., 2013, Geology, stable isotope, and U-Pb geochronology of the Mariquita porphyry copper and Lucy Cu-Mo deposits, Cananea district, Mexico: A contribution to regional exploration: Journal of Geochemical Exploration, v. 124, p. 140–154.

Ding, T.P., Valkiers, S., Wang, D.F., Bai, R.M., Zou, X.Q., Li, Y.H., Zhang, Q.L., and De Bievre, P., 2001, The $\delta^{32}S$ and $\delta^{34}S$ values and absolute $^{32}S/^{33}S$ and $^{32}S/^{34}S$ ratios of IAEA and Chinese sulfur isotope reference materials: Bulletin of Mineralogy, Petrology and Geochemistry, v. 20, p. 425–427 (in Chinese with English abs.).

Du, A.D., He, H.Y., Yin, W.N., Zhou, X.Q., Sun, Y.L., Sun, D.Z., Chen, S.Z., and Qu, W.J., 1994, The study on the analytical methods of Re-Os age for molybdenites: Acta Geologica Sinica, v. 68, p. 339–347 (in Chinese with English abs.).

Du, A.D., Wu, S.Q., Sun, D.Z., Wang, S.X., Qu, W.Q., Markey, R., Stain, H., Morgan, J., and Malinovskiy, D., 2004, Preparation and certification of Re\Os dating reference materials: Molybdenites HLP and JDC: Geostandards and Geoanalytical Research, v. 28, p. 41–52.

Eastoe, C.J., 1983, Sulfur isotope data and the nature of the hydrothermal systems at the Panguna and Frieda porphyry copper deposits, Papua New Guinea: Economic Geology, v. 78, p. 201–213.

Faure, K., and Brathwaite, R.L., 2006, Mineralogical and stable isotope studies of gold-arsenic mineralisation in the Sams Creek peralkaline porphyritic granite, South Island, New Zealand: Mineralium Deposita, v. 40, p. 802–827.

Field, C.W., 1966, Sulfur isotope abundance data, Bingham district, Utah: Economic Geology, v. 61, p. 850–871.

Field, C.W., and Gustafson, L.B., 1976, Sulfur isotopes in the porphyry copper deposit at El Salvador, Chile: Economic Geology, v. 71, p. 1533–1548.

Field, C.W., Zhang, L., Dilles, J.H., Rye, R.O., and Reed, M.H., 2005, Sulfur and oxygen isotope record in sulfate and sulfide minerals of early, deep, pre-Main Stage porphyry Cu-Mo and late Main Stage base-metal mineral deposits, Butte district, Montana: Chemical Geology, v. 215, p. 61–93.

Frei, R., 1995, Evolution of mineralizing fluid in the porphyry copper system of the Skouries deposit, Northeast Chalkidiki (Greece): Evidence from combined Pb-Sr and stable isotope data: Economic Geology, v. 90, p. 746–762.

Ge, W.C., Wu, F.Y., Zhou, C.Y., and Zhang, J.H., 2007, Porphyry Cu-Mo deposits in the eastern Xing' an-Mongolian orogenic belt: Mineralization ages and their geodynamic implications: Chinese Science Bulletin, v. 52, p. 3416–3427.

Goldfarb, R.J., Taylor, R.D., Collins, G.S., Goryachev, N.A., and Orlandini, O.F., 2013, Phanerozoic continental growth and gold metallogeny of Asia: Gondwana Research, v. 25, p. 48–102.

Hong, D.W., Wang, S.G., Xie, X.L., Zhang, J.S., and Wang, T., 2003, Metallogenic province derived from mantle sources: Nd, Sr, S and Pb isotope evidence from the Central Asian orogenic belt: Gondwana Research, v. 6, p. 711–728.

Inner Mongolian Bureau of Geology and Mineral Resources (IMBGMR), 1991, Regional geology of Inner Mongolian Autonomous region: Beijing, Geological Publishing House, 725 p. (in Chinese).

Ionov, D.A., Hoefs, J., Wedepohl, K.H., and Wiechert, U., 1992, Content and isotopic composition of sulphur in ultramafic xenoliths from central Asia: Earth and Planetary Science Letters, v. 111, p. 269–286.

Jahn, B.M., Wu, F., and Chen, B., 2000, Massive granitoid generation in Central Asia: Nd isotope evidence and implication for continental growth in the Phanerozoic: Episodes, v. 23, p. 82–92.

Jin, Y., Liu, Y.T., and Xie, Y.L., 2005, Relationship between magmatism and polymetal mineralization in Dongwuqi area, Inner Mongolia: Geology and Mineral Resources of South China, v. 21, p. 8–12 (in Chinese with English abs.).

Koval, P.V., Grebenshchikova, V.I., Lustenberg, E.E., and Henney, P.J., 1999, Database of granites in the Mongol-Okhotsk zone, Mongolia-Siberia, and its use in mineral exploration: Journal of Geochemical Exploration, v. 66, p. 199–210.

Kovalenko, V.I., Yarmolyuk, V.V., Kovach, V.P., Kotov, A.B., Kozakov, I.K., Salnikova, E.B., and Larin, A.M., 2004, Isotope provinces, mechanisms of generation and sources of the continental crust in the Central Asian mobile belt: Geological and isotopic evidence: Journal of Asian Earth Sciences, v. 23, p. 605–627.

Kovalenko, V., Yarmolyuk, V., and Bogatikov, O., 1995, Magmatism, geodynamics, and metallogeny of Central Asia: Moscow, Miko Commercial Herald Publishers, 272 p.

Lang, J.R., Guan, Y., and Eastoe, C.J., 1989, Stable isotope studies of sulfates and sulfides in the Mineral Park porphyry Cu-Mo system, Arizona: Economic Geology, v. 84, p. 650–662.

Li, H., Ye, H., Wang, X., Yang, L., and Wang, X., 2014, Geology and ore fluid geochemistry of the Jinduicheng porphyry molybdenum deposit, East Qinling, China: Journal of Asian Earth Sciences, v. 79, p. 641–654.

Li, W., Jackson, S.E., Pearson, N.J., and Graham, S., 2010, Copper isotopic zonation in the Northparkes porphyry Cu-Au deposit, SE Australia: Geochimica et Cosmochimica Acta, v. 74, p. 4078–4096.

Liu, J.M., Zhang, R., and Zhang, Q.Z., 2004, The regional metallogeny of Da Hinggan Ling, China: Earth Science Frontiers, v. 11, p. 269–277 (in Chinese with English abs.).

Liu, Y.J., and Zhou, L., 2010, Discussion on the geological characteristics and formation cause of Xiaodonggou molybdenite-lead and zinc of Inner Mongolia: Geology of Chemical Minerals, v. 32, p. 123–128 (in Chinese with English abs.).

Lüders, V., Romer, R.L., Gilg, H.A., Bodnar, R.J., Pettke, T., and Misantoni, D., 2009, A geochemical study of the Sweet Home mine, Colorado Mineral Belt, USA: Hydrothermal fluid evolution above a hypothesized granite cupola: Mineralium Deposita, v. 44, p. 415–434.

Ludwig, K.R., 2001, User's manual for Isoplot/Ex (rev. 2.49): A geochronological toolkit for Microsoft Excel: Berkeley Geochronology Center Special Publication, v. 1, p. 1–55.

Ma, X., Chen, B., and Yang, M., 2013, Magma mixing origin for the Aolunhua porphyry related to Mo-Cu mineralization, eastern Central Asian orogenic belt: Gondwana Research, v. 24, p. 1152–1171.

Meng, X.J., Hou, Z.Q., and Li, Z.Q., 2006, Sulfur and lead isotope compositions of the Qulong porphyry copper deposit, Tibet: Implications for the sources of plutons and metals in the deposit: Acta Geologica Sinica, v. 80, p. 560–569 (in Chinese with English abs.).

Mirnejad, H., Mathur, R., Hassanzadeh, J., Shafie, B., and Nourali, S., 2013, Linking Cu mineralization to host porphyry emplacement: Re-Os ages of molybdenites versus U-Pb ages of zircons and sulfur isotope compositions of pyrite and chalcopyrite from the Iju and Sarkuh porphyry deposits in Southeast Iran: Economic Geology, v. 108, p. 861–870.

Morales Ruano, S., Both, R.A., and Golding, S.D., 2002, A fluid inclusion and stable isotope study of the Moonta copper-gold deposits, South Australia: Evidence for fluid immiscibility in a magmatic hydrothermal system: Chemical Geology, v. 192, p. 211–226.

Nie, F.J., and Jiang, S.H., 2011, Geological setting and origin of Mo-W-Cu deposits in the Honggor-Shamai district, Inner Mongolia, North China: Resource Geology, v. 61, p. 344–355.

Nie, F.J., Jiang, S.H., Zhang, Y., Bai, D.M., Hu, P., Zhao, Y.Y., Zhang, W.Y., and Liu, Y., 2007, Metallogenic studies and prospecting orientation in central and eastern segments along China-Mongolia border: Beijing, Geological Publishing House, 574 p. (in Chinese).

Nie, X.L., and Hou, W.R., 2010, The discovery of the Diyanqinamu large-size Mo-Ag deposit, Inner Mongolia, and its geological significance: Acta Geoscientica Sinica, v. 31, p. 469–472 (in Chinese with English abs.).

Ohmoto, H., and Rye, R.O., 1979, Isotopes of sulfur and carbon, *in* Barnes, H.L., ed., Geochemistry of hydrothermal ore deposits, 2nd ed.: New York, Wiley, p. 509–567.

Qu, X.M., Hou, Z.Q., Zaw, K., and Li, Y.G., 2007, Characteristics and genesis of Gangdese porphyry copper deposits in the southern Tibetan Plateau: Preliminary geochemical and geochronological results: Ore Geology Reviews, v. 31, p. 205–233.

Ren, S.K., Walshe, J.L., Paterson, R.G., Both, R.A., and Andrew, A., 1995, Magmatic and hydrothermal history of the porphyry-style deposits of the Ardlethan tin field, New South Wales, Australia: Economic Geology, v. 90, p. 1620–1645.

Sarkar, S.C., Kabiraj, S., Bhattacharya, S., and Pal, A.B., 1996, Nature, origin and evolution of the granitoid-hosted early Proterozoic copper-molybdenum mineralization at Malanjkhand, Central India: Mineralium Deposita, v. 31, p. 419–431.

Seltmann, R., Mike Porter, T., and Pirajno, F., 2014, Geodynamics and metallogeny of the central Eurasian porphyry and related epithermal mineral systems: A review: Journal of Asian Earth Sciences, v. 79, p. 810–841.

Sengör, A.M.C., Natal'In, B.A., and Burtman, V.S., 1993, Evolution of the Altaid tectonic collage and Palaeozoic crustal growth in Eurasia: Nature, v. 364, p. 299–307.

Shelton, K.L., and Rye, D.M., 1982, Sulfur isotope compositions of ores from Mines Gaspe, Quebec: An example of sulfate-sulfide isotope disequilibria in ore-forming fluids with applications to other porphyry-type deposits: Economic Geology, v. 77, p. 1688–1709.

Shen, C.L., Zhang, M., Yu, X.Q., Chen, W.G., Gao, W.Y., and Zhou, W.C., 2010, New progresses in exploration of molybdenum deposits and analysis of mineralization prospect in Inner Mongolia: Geology and Exploration, v. 46, p. 561–575 (in Chinese with English abs.).

Shen, P., Shen, Y., Pan, H., Li, X.H., Dong, L., Wang, J., Zhu, H., Dai, H., and Guan, W., 2012, Geochronology and isotope geochemistry of the Baogutu porphyry copper deposit in the west Junggar region, Xinjiang, China: Journal of Asian Earth Sciences, v. 49, p. 99–115.

Smoliar, M.I., Walker, R.J., and Morgan, J.W., 1996, Re-Os ages of group IIA, IIIA, IVA, and IVB iron meteorites: Science, v. 271, p. 1099–1102.

Sotnikov, V.I., Berzina, A.N., Economou-Eliopoulos, M., and Eliopoulos, D. G., 2001, Palladium, platinum and gold distribution in porphyry Cu ± Mo deposits of Russia and Mongolia: Ore Geology Reviews, v. 18, p. 95–111.

Sotnikov, V.I., Ponomarchuk, V.A., Pertseva, A.P., Berzina, A.P., Berzina, A.N., and Gimon, V.O., 2004, Evolution of sulfur isotopes in porphyry Cu-Mo ore-magmatic systems of Siberia and Mongolia: Russian Geology and Geophysics, v. 45, p. 963–974.

Stacey, J.S., and Kramers, J.D., 1975, Approximation of terrestrial lead isotope evolution by a two-stage model: Earth and Planetary Science Letters, v. 26, p. 207–221.

Stein, H.J., and Hannah, J.L., 1985, Movement and origin of ore fluids in Climax-type systems: Geology, v. 13, p. 469–474.

Sun, H.R., Huang, Z.L., Li, W.B., Leng, C.B., Ma, D. Y., and Zhang, X.C., 2014, Chronology, geochemistry and Sr-Nd isotope studies of Jurassic intrusions in the Diyanqinamu porphyry Mo mine, central Inner Mongolia, China: Journal of Asian Earth Sciences, v. 88, p. 85–97.

Sun, J.G., Sun, Y., Xing, S.W., Zhao, K.Q., Zhang, Z.J., Bai, L.A., Ma, Y.B., and Liu, Y.S., 2012, Genetic types, ore-forming age and geodynamic setting of endogenic molybdenum deposits in the eastern edge of Xing-Meng orogenic belt: Acta Petrologic Sinica, v. 28, p. 1317–1332 (in Chinese with English abs.).

Todt, W., Cliff, R.A., Hanser, A., and Hofmann, A.W., 1996, Evaluation of a ^{202}Pb-^{205}Pb double spike for high-precision lead isotope analysis, *in* Hart, S.R., and Basu, A., eds., Earth processes: Reading the isotope code: Washington, American Geophysical Union, v. 95, p. 429–437

Ueda, A., and Sakai, H., 1984, Sulfur isotope study of Quaternary volcanic rocks from the Japanese Islands arc: Geochimica et Cosmochimica Acta, v. 48, p. 1837–1848.

Valencia, V.A., Eastoe, C., Ruiz, J., Ochoa-Landin, L., Gehrels, G., Gonzalez-Leon, C., Barra, F., and Espinoza, E., 2008, Hydrothermal evolution of the porphyry copper deposit at La Caridad, Sonora, Mexico, and the relationship with a neighboring high-sulfidation epithermal deposit: Economic Geology, v. 103, p. 473–491.

Wan, B., Hegner, E., Zhang, L., Rocholl, A., Chen, Z., Wu, H., and Chen, F., 2009, Rb-Sr geochronology of chalcopyrite from the Chehugou porphyry Mo-Cu deposit (Northeast China) and geochemical constraints on the origin of hosting granites: Economic Geology, v. 104, p. 351–363.

Wang, S., Zhang, X., Leng, C., and Qin, C., 2007, A tentative study of ore geochemistry and ore-forming mechanism of Pulang porphyry copper deposit in Zhongdian, northwestern Yunnan: Mineral Deposits, v. 26, p. 277–288 (in Chinese with English abs.).

Wareham, C.D., Rice, C.M., Boyce, A.J., and Rogers, G., 1998, S, C, Sr, and Pb sources in the Pliocene Silver Creek porphyry, Mo system Rio, Colorado: Economic Geology, v. 93, p. 32–46.

Watanabe, Y., and Hedenquist, J.W., 2001, Mineralogic and stable isotope zonation at the surface over the El Salvador porphyry copper deposit, Chile: Economic Geology, v. 96, p. 1775–1797.

Wilson, A.J., Cooke, D.R., Harper, B.J., and Deyell, C.L., 2007, Sulfur isotopic zonation in the Cadia district, southeastern Australia: Exploration significance and implications for the genesis of alkalic porphyry gold-copper deposits: Mineralium Deposita, v. 42, p. 465–487.

Windley, B.F., Alexeiev, D., Xiao, W., Kröner, A., and Badarch, G., 2007, Tectonic models for accretion of the Central Asian orogenic belt: Journal of the Geological Society, v. 164, p. 31–47.

Wu, F.Y., Jahn, B.M., Wilde, S., and Sun, D.Y., 2000, Phanerozoic crustal growth: U-Pb and Sr-Nd isotopic evidence from the granites in northeastern China: Tectonophysics, v. 328, p. 89–113.

Wu, H.Y., Zhang, L.C., Chen, Z.G., and Wan, B., 2008, Geochemistries, tectonic setting and mineralization potentiality of the ore-bearing monzogranite in the Kulitu molybdenum (copper) deposit of Xar moron metallogetic belt, Inner Mongolia: Acta Petrologica Sinica, v. 24, p. 867–878 (in Chinese with English abs.).

Wu, H., Zhang, L., Wan, B., Chen, Z., Xiang, P., Pirajno, F., Du, A., and Qu, W., 2011, Re-Os and $^{40}Ar/^{39}Ar$ ages of the Jiguanshan porphyry Mo deposit, Xilamulun metallogenic belt, NE China, and constraints on mineralization events: Mineralium Deposita, v. 46, p. 171–185.

Xiao, W., Windley, B.F., Hao, J., and Zhai, M., 2003, Accretion leading to collision and the Permian Solonker suture, Inner Mongolia, China: Termination of the central Asian orogenic belt: Tectonics, v. 22, p. DOI: 10.1029/2002TC001484.

Xiao, W., Kroner, A., and Windley, B., 2009, Geodynamic evolution of Central Asia in the Paleozoic and Mesozoic: International Journal of Earth Sciences, v. 98, p. 1185-1188.

Yan, H., Huang, F.X., Sun, H., Zhao, L.Q., Zhang, Y., Zhang, H., Li, S.Z., Liu, F.F., and Wang, J.S., 2012, A model for alteration zoning of hydrothermal mineralization based on Surpace software for the Diyanqinamu Mo mine district, Inner Mongolia: Geology and Exploration, v. 48, p. 932–939 (in Chinese with English abs.).

Ying, L.J., Zheng, W.B., Wang, W.P., Leng, Q.F., and Ding, S., 2013, Stable isotopes geochemistry of the Jiama copper polymetallic deposit in Tibet: Acta Geoscientica Sinica, v. 33, p. 519–527 (in Chinese with English abs.).

Zhang, H.T., So, C.S., and Yun, S.T., 1999, Regional geologic setting and metallogenesis of central Inner Mongolia, China: Guides for exploration of mesothermal gold deposits: Ore Geology Reviews, v. 14, p. 129–146.

Zhang, L.C., Wu, H.Y., Wan, B., and Chen, Z.G., 2009, Ages and geodynamic settings of Xilamulun Mo-Cu metallogenic belt in the northern part of the North China craton: Gondwana Research, v. 16, p. 243–254.

Zhang, W.Y., 2008, Magmatic activity and metallogeny of Dong Ujimqin Banner, Inner Mongolia: Chinese Academy of Geological Science, 131 p. (in Chinese).

Zhao, G.L., Yang, G.L., Fu, J.Y., Wang, Z., Fu, J.Y., and Yang, Y.Z., 1989, Mesozoic volcanic rocks in central and southern Da Hinggan Ling Range: Beijing, Science and Technology Publishing House, 260 p. (in Chinese with English abs.)

Zhao, Y.M, Wang, D.W., and Zhang, D.Q., 1994, Metallogenic geological conditions and prospecting model for copper polymetallic deposits in east south part of Inner Mongolia: Beijing, Seismological Publishing House, 234 p. (in Chinese).

Zhou, Z.H., Mao, J.W., and Lyckberg, P., 2012, Geochronology and isotopic geochemistry of the A-type granites from the Huanggang Sn-Fe deposit, southern Great Hinggan Range, NE China: Implication for their origin and tectonic setting: Journal of Asian Earth Sciences, v. 49, p. 272–286.

Zorin, Y.A., Zorina, L.D., Spiridonov, A.M., and Rutshtein, I.G., 2001, Geodynamic setting of gold deposits in Eastern and Central Trans-Baikal (Chita region, Russia): Ore Geology Reviews, v. 17, p. 215–232.